

High-dimensional Grouped-regression using Bayesian Sparse Projection-posterior

Samhita Pal, Subhashis Ghoshal

Abstract

We consider a novel Bayesian approach to estimation, uncertainty quantification, and variable selection for a high-dimensional linear regression model under sparsity. The number of predictors can be nearly exponentially large relative to the sample size. We put a conjugate normal prior initially disregarding sparsity, but for making an inference, instead of the original multivariate normal posterior, we use the posterior distribution induced by a map transforming the vector of regression coefficients to a sparse vector obtained by minimizing the sum of squares of deviations plus a suitably scaled ℓ_1 -penalty on the vector. We show that the resulting sparse projection-posterior distribution contracts around the true value of the parameter at the optimal rate adapted to the sparsity of the vector. We show that the true sparsity structure gets a large sparse projection-posterior probability. We further show that an appropriately recentered credible ball has the correct asymptotic frequentist coverage. Finally, we describe how the computational burden can be distributed to many machines, each dealing with only a small fraction of the whole dataset. We conduct a comprehensive simulation study under a variety of settings and found that the proposed method performs well for finite sample sizes. We also apply the method to several real datasets, including the ADNI data, and compare its performance with the state-of-the-art methods. We implemented the method in the R package called `sparseProj`, and all computations have been carried out using this package.

1 Introduction

High-dimensional linear regression models with numerous predictors, potentially exceeding the observations in number, have garnered significant research interest. Most predictors remain inactive in such models, leading to sparsity in the regression coefficient vector. This feature enables reliable estimation of coefficients by leveraging the underlying low-dimensional structure. Introducing a penalty function to the objective

function is a common approach to dealing with such problems, encouraging the minimizer to yield sparser solutions. The popular method LASSO (Tibshirani, 1996; Zhang and Huang, 2008) enforces an ℓ_1 -norm constraint on the coefficient vectors, resulting in exact zeros at some coordinates. Variations of the LASSO include the Minimax Concave Penalty (MCP) (Zhang, 2010), Smoothly Clipped Absolute Deviation (SCAD) (Fan and Li, 2001), Dantzig selector (Candes and Tao, 2007), adaptive LASSO (Zou, 2006), non-negative garrotte (Breiman, 1995; Yuan and Lin, 2007) estimators. Earlier research explored LASSO’s asymptotic properties, such as consistency and limiting distribution, in fixed-dimensional settings (Fu and Knight, 2000). A bootstrap LASSO was introduced, but Chatterjee and Lahiri (2010) demonstrated that it lacks consistency when one or more components of the coefficient vector are zero.

Bayesian methods for high-dimensional linear models under sparsity have been also developed. The Bayesian LASSO (Park and Casella, 2008; Hans, 2009) employs a Laplace prior for each coefficient. While the posterior mode is the LASSO, the posterior distribution is not supported on sparse vectors and fails to concentrate near the true parameter vector. A spike-and-slab prior (Mitchell and Beauchamp, 1988; Ishwaran and Rao, 2005) can address the issue by introducing sparsity in coefficients through a point mass at zero. It automatically selects a smaller subset of predictors as the active set in each posterior draw of the regression coefficients, resulting in multiple models in the posterior. Each model corresponds to an active predictor set; hence, computing all model posterior probabilities is very intensive. The Stochastic Search Variable Selection (SSVS) method (George and McCulloch, 1993) uses Gibbs sampling to address the issue, but it is still a slow process. Continuous shrinkage priors replace a spike and slab mixture with a single density using a global scale parameter across all components to obtain a thick tail and a local scale parameter to create a high concentration at zero. Hence, they are also referred to as global-local priors. Some notable continuous shrinkage priors include the horseshoe (Carvalho et al., 2009), normal-gamma (Brown and Griffin, 2010), double-Pareto (Armagan et al., 2013), Dirichlet-Laplace (Bhattacharya et al., 2015), and R2-D2 (Zhang et al., 2022).

Variational inference (Wainwright et al., 2008) provides a computationally faster method to approximately compute posterior distributions through optimization. Ray and Szabó (2022); Ormerod et al. (2017); Huang et al. (2016) studied the mean-field spike and slab variational Bayes approximation for high-dimensional linear regression, whereas Mukherjee and Sen (2022) studied the naive mean-field approximation to the posterior distribution arising from product priors. A general α -variational inference technique for the high-dimensional linear model under sparsity was provided in Yang et al. (2020). These variational methods also possess estimation or selection consistency. Moreover, Zhang and Gao (2020) extensively studied convergence rates of these

variational Bayes methods in the high-dimensional linear regression setting. The paper [Han and Yang \(2019\)](#) conducted a non-asymptotic analysis on the approximation of the posterior distributions in linear models involving latent variables. However, to our knowledge, uncertainty quantification of these methods has not been investigated, except for [Yang and Martin \(2020\)](#) and [Bai et al. \(2020\)](#). The former considered posterior distributions obtained by updating an appropriate empirically-centered Gaussian prior and showed valid frequentist coverage of their credible balls under the orthogonal design matrix. On the other hand, the latter proposed a variational approach for heavy-tailed shrinkage priors but failed to show coverage.

Some authors also studied the asymptotic properties of posterior distributions in high-dimensional linear regression models. The paper [Castillo et al. \(2015\)](#) obtained the posterior contraction rate of a spike-and-slab prior with a Laplace slab akin to the LASSO’s convergence rate and also showed that if signals are sufficiently strong, then the posterior selects the model with the correct set of predictors with high probability. They stressed the importance of the tail thickness of the slab density to prevent excessive shrinkage that may compromise the posterior contraction rate. Using an empirical Bayes approach to select the prior mean of the slab distribution instead of setting it to zero, [Belitser and Ghosal \(2020\)](#) showed that optimal posterior contraction can be obtained using a conjugate normal slab distribution. Posterior contraction and variable selection properties of continuous shrinkage priors were established by [Song and Liang \(2017\)](#).

In this paper, we introduce an innovative Bayesian approach to obtain a posterior distribution supported on sparse subspaces using a conjugate prior on the regression coefficient, which is easy to compute, and the posterior has optimal contraction and variable selection properties. Moreover, credible regions with asymptotically correct frequentist coverage can be obtained from the resulting posterior distribution. This approach differs from traditional Bayesian methods in that a restriction like sparsity is not imposed in the prior. Thus, conjugate priors may be used, significantly simplifying the analysis. The inference is conducted by the induced posterior distribution of a sparsity-generating map, immersing full vectors in a sparse region. The resulting “sparse projection-posterior” samples are easily obtained by conjugate sampling corrected by an optimization step. The idea of using such an immersion map to transform sample draws from a conjugate posterior distribution on an unrestricted parameter space to the desirable constricted space was used previously in the contexts of monotone shape regression [Lin and Dunson \(2014\)](#); [Chakraborty and Ghosal \(2021a,b\)](#); [Wang and Ghosal \(2023\)](#) and differential equation models [Bhaumik and Ghosal \(2015, 2017\)](#); [Bhaumik et al. \(2022\)](#).

Under the standard conditions of bounded predictor variables and compatibility

conditions used for LASSO’s convergence, we demonstrate that the sparse projection-posterior contracts at the same rate as the LASSO. For the LASSO, consistency of variable selection is established assuming the beta-min condition and the ‘irrepresentable’ condition (Wainwright, 2009; Yuan and Lin, 2006; Meinshausen and Yu, 2009). We show that, under these conditions, the sparse projection-posterior probability of the model consisting of the true set of active predictors approaches one. A notable limitation of LASSO is its inability to provide standard errors and confidence regions for coefficients with estimated zeros. A debiasing technique was employed to obtain confidence intervals (Zhang and Zhang, 2014; van de Geer et al., 2014; Javanmard and Montanari, 2018) at the expense of sparsity. Chatterjee and Lahiri (2011) developed a modified residual bootstrap technique for constructing confidence sets with good coverage properties. Various aspects of coverage in the sparse linear regression setting were studied by Nickl and van de Geer (2013); Cai and Guo (2017). While Bayesian methods hold promise for quantifying uncertainty, adjustments are often needed to match their credibility with asymptotic frequentist coverage. The article Belitser and Ghosal (2020) showed that a Bayesian credible ball of the optimal size adapted to the sparsity of the regression coefficient has adequate frequentist coverage at all parameter points satisfying an *excessive bias restriction* condition. We show that a recentered sparse projection-posterior can construct credible intervals with valid frequentist coverage for each regression coefficient. This is equivalent to employing a debiased version of the original immersion map only for this purpose. Moreover, the sparse projection-posterior method is tailored for distributed computing, which is typically impossible for traditional Bayesian methods. Its unique approach avoids MCMC sampling, requiring only conjugate Gaussian prior draws, promising faster results.

Using an immersion map adds more flexibility to the Bayesian paradigm, similar to other extensions such as the empirical Bayes or the variational method. The variational approach finds a projection of the posterior distribution within a given class of distributions, thus transforming the original posterior distribution to a related distribution. In this sense, the sparse projection-posterior, or more generally, an “immersion posterior” induced by an immersion map relevant to the context, is conceptually similar to the variational approach. In both contexts, the transformation is obtained by an optimization step. The main difference is that, in the variational method, the optimization is done at the distributional level, while in the immersion posterior approach, the optimization is on the arguments of the distribution. Further, in the variational approach, the original posterior distribution is not calculated, and the variational posterior is intended to approximate it. However, in the immersion posterior approach, a simple unrestricted posterior is computed typically through conjugacy, but it is never intended for inference. The optimization step in the immersion posterior approach is

typically non-iterative and more straightforward than in the variational method. This results in a more explicit description of the immersion posterior that allows for studying finer properties like model selection and coverage. Finally, we note that even though the variational posterior was initially intended to be an approximation to the original posterior, such approximation results are not available, so the variational posterior is eventually considered as an alternative random measure to be used to make an inference instead of the actual posterior distribution. This also prompts the need to study the convergence properties of the variational posterior. The immersion posterior provides another typically simpler alternative with many desirable convergence properties.

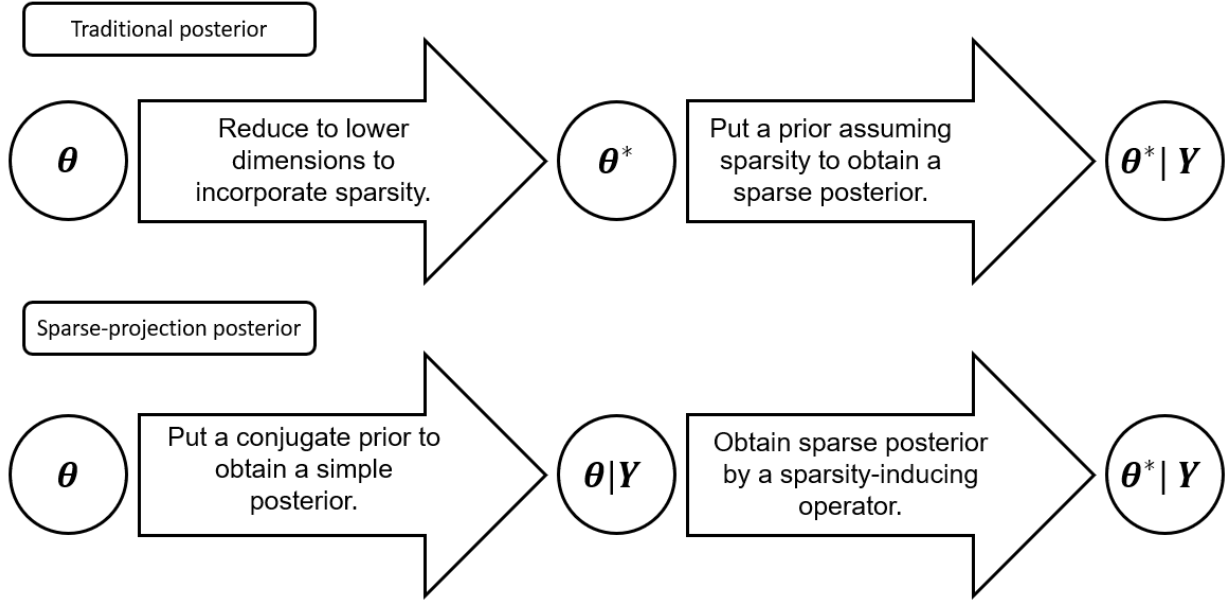
The paper is organized as follows. In Section 2, we introduce the proposed novel Bayesian approach to inference for a high-dimensional linear regression problem using the sparse projection-posterior distribution. Its contraction rate, variable selection, and coverage properties are established in Section 3, followed by numerical results in Section 4. A discussion summarizing the aspects of the proposed method is presented in Section 7. The proofs of the theorems are provided in Supplement 1 of the Appendix section. A recipe for distributed computing suitable for handling large datasets and addressing privacy concerns by distributing the computation in several local machines is presented in Section 2.5, while Supplement 3 contains some additional numerical results.

2 Methodology

2.1 Motivation

For a high-dimensional linear regression, constructing a prior on the regression coefficients with support on a sparse domain leads to a posterior that is hard to compute and analyze theoretically because of the varying restrictions imposed by sparsity. The procedure would be much easier to compute and study if the sparsity restrictions were not imposed before sampling from the posterior, but instead, if a correction map was used to convert a posterior sample to a sparse vector. This can be done using a sparsity-inducing map on the full posterior from the entire parameter space. This is not a projection map because of the presence of a penalty term in its objective function, but the resulting induced *sparse projection-posterior* may be viewed as an immersion posterior in the sense of Wang and Ghosal (2023). A natural choice of a sparse transformation that maps the whole parameter space to a sparser subspace is obtained by minimizing the sum of a weighted squared ℓ_2 -norm and a standard sparsity-inducing penalty, such as the ℓ_1 -penalty. The new method can be thought of as obtained by switching the order of operation of imposing the sparsity restriction and posterior up-

dating in a usual Bayesian method for high-dimensional regression, as schematically demonstrated below:



This helps bypass the hassle of MCMC, making computations quite efficient. However, in the end, both approaches lead to a data-dependent probability measure on the derived parameter space to make an inference about the parameter. Another advantage of this method is that the mapping can simultaneously be done with different tuning parameters λ per the study’s requirement or purpose. A smaller value of λ can be used if the main goal is estimation or prediction, whereas a much larger value of the tuning parameter will be needed for consistent model selection. Optimal frequentist properties guide the choice of these maps.

Another interpretation of the sparse projection-posterior can be given in terms of a “super-parameter model” and a misspecified likelihood. We may view the true parameter θ^0 as a sparse projection $\theta^0 = \iota(\beta^0)$ of a “super-parameter” β^0 with no sparsity in its entries. Thus a vanilla conjugate prior can be used to make an inference on β , using the misspecified likelihood obtained from the model $\mathbf{Y} \sim \mathcal{N}_n(\mathbf{X}\beta, \sigma^2\mathbf{I}_n)$, instead of the correct model $\mathbf{Y} \sim \mathcal{N}_n(\mathbf{X}\theta, \sigma^2\mathbf{I}_n)$. Since an inference on β is not of interest, but that on θ is, we use the distribution induced by the map ι from the conjugate posterior for β .

Finally, an exciting feature of the proposed sparse projection-posterior approach is that the computation can be divided among several computers, as described in Subsection 2.5. This property allows for handling very big datasets or datasets with privacy concerns without requiring the storage of the data in one machine.

2.2 Model and Notations

We consider the linear regression model $\mathbf{Y} = \mathbf{X}\boldsymbol{\theta} + \boldsymbol{\varepsilon}$, where $\mathbf{X} \in \mathbb{R}^n \times \mathbb{R}^p$ is the standardized design matrix, $\mathbf{Y} \in \mathbb{R}^n$ be the response vector, the random noise $\boldsymbol{\varepsilon} \in \mathbb{R}^n$ is distributed as $\mathcal{N}_n(0, \sigma^2 \mathbf{I}_n)$ for some $\sigma > 0$, and $\boldsymbol{\theta} \in \mathbb{R}^p$ is the vector of regression coefficients. The model dimension p can grow with n and be much larger than n . The design matrix \mathbf{X} is standardized so that each column has Euclidean norm n .

Let $\boldsymbol{\theta}^0$ denote the true value of the coefficient vector. Let $S_0 = \{j : \theta_j^0 \neq 0\}$ be the active set corresponding to $\boldsymbol{\theta}^0$ and s_0 be the cardinality of S_0 , that is, the number of active predictors in the model, known as the sparsity index. Probability statements under the true distribution will be indicated by $\mathbb{P}_{\boldsymbol{\theta}^0}$. We write $\mathbf{C}_n = n^{-1} \mathbf{X}^T \mathbf{X}$ for the sample covariance matrix. For notational convenience, we assume without loss of generality that the first s_0 variables, denoted by $\mathbf{X}_{(1)}$, are active and the true values of the coefficients corresponding to the last $p - s_0$ variables, denoted by $\mathbf{X}_{(2)}$, equal zero. Then \mathbf{C}_n can be split as

$$\mathbf{C}_n = \begin{bmatrix} \mathbf{C}_{n(11)} & \mathbf{C}_{n(12)} \\ \mathbf{C}_{n(21)} & \mathbf{C}_{n(22)} \end{bmatrix} = \frac{1}{n} \begin{bmatrix} \mathbf{X}_{(1)}^T \mathbf{X}_{(1)} & \mathbf{X}_{(1)}^T \mathbf{X}_{(2)} \\ \mathbf{X}_{(2)}^T \mathbf{X}_{(1)} & \mathbf{X}_{(2)}^T \mathbf{X}_{(2)} \end{bmatrix}. \quad (2.1)$$

We shall use the following notations throughout the paper. The symbol $\|\mathbf{a}\|_q$ stands for the q -norm of the vector $\mathbf{a} \in \mathbb{R}^d$ given by $(\sum_{i=1}^d |a_i|^q)^{1/q}$. If $q = 2$, which corresponds to the usual Euclidean norm, we shall generally drop the index 2 from the notation. For a $d_1 \times d_2$ -matrix \mathbf{M} , by \mathbf{M}_A , we denote the submatrix containing the columns corresponding to a given set $A \subset \{1, 2, \dots, d_2\}$. In particular, when $A = \{j\}$ for some $j \in \{1, \dots, p\}$, we write $\mathbf{M}^{(j)}$ for the j th column of \mathbf{M} and write $\mathbf{M}^{(-j)}$ for the submatrix of \mathbf{M} without the j th column. A random variable X_n weakly converges to X is denoted by $X_n \rightsquigarrow X$, and the \gg or \ll signs are used to describe much larger or much smaller comparisons, respectively. Let $a_n = \mathcal{O}(b_n)$ mean the sequence a_n is bounded by a multiple of b_n , $a_n \asymp b_n$ mean both $a_n = \mathcal{O}(b_n)$ and $b_n = \mathcal{O}(a_n)$. We use $\|\mathbf{M}\|_F$ to denote the Frobenius norm of the matrix $\mathbf{M} \in \mathbb{R}^{m \times n}$ defined by $\sqrt{\sum_{i=1}^m \sum_{j=1}^n |M_{ij}|^2}$ and an L_q norm of the matrix is the vector-induced norm defined by $\|\mathbf{M}\|_q = \sup_{\mathbf{x} \neq \mathbf{0}} \|\mathbf{M}\mathbf{x}\|_p / \|\mathbf{x}\|_p$.

2.3 Prior Specification and Posterior Distribution

We now specify the prior distribution for the parameters. Given $\sigma > 0$, let $\boldsymbol{\theta}$ be given the conjugate prior $\boldsymbol{\theta} | \sigma \sim \mathcal{N}_p(\mathbf{0}, a_n^{-1} \sigma^2 \mathbf{I}_p)$ for some constant a_n depending on n . Then, the posterior distribution of the parameter vector given σ can then be easily computed

as

$$\boldsymbol{\theta} | (\mathbf{X}, \mathbf{Y}, \sigma) \sim \mathcal{N}_p(\hat{\boldsymbol{\theta}}^R, \sigma^2(\mathbf{X}^T \mathbf{X} + a_n \mathbf{I}_p)^{-1}), \quad (2.2)$$

where the posterior mean is defined as $\hat{\boldsymbol{\theta}}^R := (\mathbf{X}^T \mathbf{X} + a_n \mathbf{I}_p)^{-1} \mathbf{X}^T \mathbf{Y}$, owing to its resemblance with the ridge-regression estimator with penalty a_n . The prior choice made here does not take into account the sparsity of the coefficient vector, and, as a result, the obtained posterior does not lead to sparse samples of the parameter of interest. Sparsity is introduced in the next step, where posterior samples of dense vectors are projected to a lower-dimensional space using a sparsity-inducing map, say $f : \mathbb{R}^p \mapsto \mathbb{R}^d$, $d < p$, such that the unrelated components are zeroed out, giving rise to sparse posterior samples as desired.

The marginal likelihood for σ given by $\ell(\sigma) \propto \sigma^{-n} \exp[-\mathbf{Y}^T (\mathbf{I}_n + a_n \mathbf{X} \mathbf{X}^T)^{-1} \mathbf{Y} / (2\sigma^2)]$ is obtained from the marginal distribution $\mathbf{Y} \sim \mathcal{N}_n(\mathbf{0}, \sigma^2(\mathbf{I}_n + a_n \mathbf{X} \mathbf{X}^T))$. An inverse-Gamma prior is conjugate to this likelihood. However, it will be seen that the resulting posterior is inconsistent if p is not small relative to n . In Subsection 3.4, we rectify it using an immersion map.

2.4 Sparse Projection

To transform dense posterior samples to confine to a space with the desired sparsity, we apply a map

$$f : \boldsymbol{\theta} \mapsto \boldsymbol{\theta}^* = \arg \min_{\mathbf{u}} \{L(\boldsymbol{\theta}, \mathbf{u}) + \lambda_n \mathcal{P}(\mathbf{u})\},$$

where L is a loss function, λ_n is a tuning parameter depending on n and $\mathcal{P}(\cdot)$ is a penalty function that enforces sparsity of the solution, and the extent of sparsity depends on the choice of λ_n . Our choice of the loss tries to capture the effect of the departure of $\mathbf{X}\boldsymbol{\theta}^*$ from $\mathbf{X}\boldsymbol{\theta}$, leading to the squared error loss $L(\boldsymbol{\theta}, \mathbf{u}) = n^{-1} \|\mathbf{X}\boldsymbol{\theta} - \mathbf{X}\mathbf{u}\|^2$, although a more general choice $(\boldsymbol{\theta} - \mathbf{u})^T \mathbf{D}(\boldsymbol{\theta} - \mathbf{u})$ is also sensible. We choose $\mathcal{P}(\mathbf{u}) = \|\mathbf{u}\|_1$, the LASSO penalty, but other choices will also meet the intent. The posterior distribution of $\mathbf{X}\boldsymbol{\theta}$ given σ is given by

$$\mathcal{N}_n(\mathbf{X}\hat{\boldsymbol{\theta}}^R, \sigma^2 \mathbf{H}(a_n)), \quad \mathbf{H}(a_n) = \mathbf{X}(\mathbf{X}^T \mathbf{X} + a_n \mathbf{I}_p)^{-1} \mathbf{X}^T. \quad (2.3)$$

Unlike the hat matrix in the formula for the least square estimator, $\mathbf{H}(a_n)$ is not a projection matrix. The posterior distribution of $\boldsymbol{\eta} = \mathbf{X}\boldsymbol{\theta} - \mathbf{X}\boldsymbol{\theta}^0$ is also Gaussian with the same variance, but with mean $\boldsymbol{\mu} = \mathbf{X}(\hat{\boldsymbol{\theta}}^R - \boldsymbol{\theta}^0)$. For a given draw $\boldsymbol{\theta}$ from its posterior distribution given σ , the sparse projection map $\boldsymbol{\theta} \mapsto \boldsymbol{\theta}^*$ is given by

$$\boldsymbol{\theta}^* = \arg \min_{\mathbf{u}} \{n^{-1} \|\mathbf{X}\boldsymbol{\theta} - \mathbf{X}\mathbf{u}\|^2 + \lambda_n \|\mathbf{u}\|_1\}. \quad (2.4)$$

It should be noted here that the map described in (2.4) is a specific choice, and the theories developed later in this paper are based on this choice. There could be several other combinations of loss functions and penalties that will guide the theoretical results. For our map, the sparse projection-posterior for $\boldsymbol{\theta}$ can be described as follows. Let σ be a draw from the marginal posterior for σ and let $\sigma^* = \iota(\sigma)$, the image under the immersion map ι for σ described in Subsection 3.4. Then $\boldsymbol{\theta}$ is drawn from $\mathcal{N}_p((\mathbf{X}^T \mathbf{X} + a_n \mathbf{I}_p)^{-1} \mathbf{X}^T \mathbf{Y}, (\sigma^*)^2 (\mathbf{X}^T \mathbf{X} + a_n \mathbf{I}_p)^{-1})$ and mapped to $\boldsymbol{\theta}^*$ through the sparse projection map. The resulting induced posterior is used to make inferences. The next section establishes its convergence, selection, and uncertainty quantification properties. The sampling scheme of the sparse projection-posterior method is described in Algorithm 1.

Algorithm 1: Projection-posterior for $\boldsymbol{\theta}$

Step 1: Draw σ from the marginal posterior for σ and let the image under the immersion map for σ be $\sigma^* = \iota(\sigma)$.

Step 2: Draw $\boldsymbol{\theta}$ from the posterior $\mathcal{N}_p(\hat{\boldsymbol{\theta}}^R, (\sigma^*)^2 (\mathbf{X}^T \mathbf{X} + a_n \mathbf{I}_p)^{-1})$.

Step 3: Map to $\boldsymbol{\theta}^*$ through the map $\boldsymbol{\theta}^* = \arg \min_{\mathbf{u}} \{n^{-1} \|\mathbf{X}\boldsymbol{\theta} - \mathbf{X}\mathbf{u}\|^2 + \lambda_n \|\mathbf{u}\|_1\}$.

2.5 Distributed Computing

Frequently, enhanced computational speed involves using multiple computers. Sometimes, it is essential due to enormous data sizes, making single-machine storage impossible, or privacy concerns prohibiting raw data transfer. The typical parallelization approach divides data into subsets processed concurrently on various processors. While this speeds up operations, communication costs hinder its effectiveness. Techniques have emerged to minimize communication by merging outcomes only in the final phase, resulting in simpler and faster algorithms. The challenge lies in designing nearly communication-free algorithms that match the statistical correctness of the concurrent methods on the complete dataset at a significantly reduced computational cost. In our context, when distributed over several computers, communication is only required in one step, where the necessary pieces are aggregated to obtain the required quantity. Suppose the data is divided into m machines that collect (or receive) n_1, \dots, n_m data units respectively, where $\sum_{j=1}^m n_j = n$. Let $(\mathbf{X}_j, \mathbf{Y}_j)$ denote the data units in the j th machine in the vector form, $j = 1, \dots, m$, while (\mathbf{X}, \mathbf{Y}) stand for the entire set of data. Clearly, $\mathbf{X}^T \mathbf{X} = \sum_{j=1}^m \mathbf{X}_j^T \mathbf{X}_j$ and $\mathbf{X}^T \mathbf{Y} = \sum_{j=1}^m \mathbf{X}_j^T \mathbf{Y}_j$. Since $\mathbf{X}_j^T \mathbf{X}_j$ and $\mathbf{X}_j^T \mathbf{Y}_j$ can be computed in the j th computer without communicating the entire raw data of the j th segment, the central computer can compute $\mathbf{X}^T \mathbf{X}$ and $\mathbf{X}^T \mathbf{Y}$ and hence draw samples from (2.2) and that of the marginal posterior distribution of σ ,

which may be corrected by an immersion map as discussed earlier. It may be noted that the auxiliary computers perform computations only once and then communicate the summary to the central processor, where all other computations, including matrix inversion, sample draws, and optimization steps, are executed. The inversion should be done by the singular value decomposition of \mathbf{X} .

It is to be noted that the distributed algorithm computes the same posterior, and hence, no new results about its asymptotic properties are needed for its justification. The sparse projection-posterior can be computed through the distributed computation technique, making it unique among Bayesian methods or their modifications. None of the available Bayesian methods, including those based on spike-and-slab or continuous shrinkage priors, are compatible with distributed computing.

3 Main Results

Below, we provide results on the contraction of the posterior at the true value of the parameter and consistency of variable selection. The set of assumptions required for the corresponding results is introduced immediately preceding the results. The assumptions made for the projection-posterior approach are closely related to those used to derive the convergence properties of the LASSO. It should be kept in mind that the assumptions can be changed as per the choice of the penalty for similar posterior convergence results to hold if one chooses to work with any other projection map.

3.1 Consistency

Definition 3.1. The posterior distribution $\Pi(\cdot|\mathbf{Y})$ is said to be estimation consistent (respectively, prediction consistent) at the true value $\boldsymbol{\theta}^0$ of the parameter $\boldsymbol{\theta}$ if for all $\epsilon > 0$, $\Pi(\|\boldsymbol{\theta} - \boldsymbol{\theta}^0\| > \epsilon|\mathbf{Y}) \rightarrow 0$ (respectively, $\Pi(\|\mathbf{X}\boldsymbol{\theta} - \mathbf{X}\boldsymbol{\theta}^0\| > \epsilon|\mathbf{Y}) \rightarrow 0$) in probability under $\boldsymbol{\theta}^0$.

The posterior distribution $\Pi(\cdot|\mathbf{Y})$ is said to contract at the rate ϵ_n at $\boldsymbol{\theta}^0$ if for any sequence $M_n \rightarrow \infty$, $\Pi(\|\boldsymbol{\theta} - \boldsymbol{\theta}^0\| > M_n\epsilon_n|\mathbf{Y}) \rightarrow 0$ in probability under $\boldsymbol{\theta}^0$.

The posterior distribution $\Pi(\cdot|\mathbf{Y})$ is said to be selection consistent if $\Pi(\{j : \boldsymbol{\theta}_j \neq 0\} = \{j : \boldsymbol{\theta}_{0j} \neq 0\}|\mathbf{Y}) \rightarrow 1$ in probability under $\boldsymbol{\theta}^0$. The posterior distribution $\Pi(\cdot|\mathbf{Y})$ is said to be sign-consistent if $\Pi(\{\text{sign}(\boldsymbol{\theta}) = \text{sign}(\boldsymbol{\theta}^0)\}|\mathbf{Y}) \rightarrow 1$ in probability under $\boldsymbol{\theta}^0$, where $\text{sign}(x) = 1, 0, -1$ respectively for $x > 0$, $x = 0$ and $x < 0$, and the function is applied coordinate-wise for a vector. Sign consistency is stronger than selection consistency because it correctly obtains the set of active predictors and captures the signs of the non-zero regression coefficients.

3.1.1 Estimation and Prediction Consistency

Define the prediction risk of $\boldsymbol{\theta}^*$ to be $n^{-1}\|\mathbf{X}(\boldsymbol{\theta}^* - \boldsymbol{\theta}^0)\|^2$ and measure the closeness between the sparse projection $\boldsymbol{\theta}^*$ and the true coefficients by the ℓ_1 -error of the estimated coefficients $\|\boldsymbol{\theta}^* - \boldsymbol{\theta}^0\|_1 = \sum_{j=1}^p |\boldsymbol{\theta}_j^* - \boldsymbol{\theta}_j^0|$. Theorem 3.1 below demonstrates that under a compatibility condition used for the LASSO, the posterior probability of the sparse projection $\boldsymbol{\theta}^*$ will concentrate around the true value $\boldsymbol{\theta}^0$, and bound the prediction rate under the following assumptions.

Assumption 3.1 (Bounded design condition). *The predictor variables are bounded, that is, there exists $M_1 > 0$ such that $|x_{ij}| \leq M_1$ for all $i = 1, \dots, n$, $j = 1, \dots, p$.*

The condition is automatically met if we standardize the design points.

Assumption 3.2 (Compatibility condition). *For $S \subset \{1, 2, \dots, p\}$, the set of predictors \mathbf{X} is said to satisfy the compatibility condition at set S if*

$$\|\mathbf{v}_S\|_1^2 \leq \frac{s_0}{\phi_0^2} \frac{1}{n} \|\mathbf{X}\mathbf{v}\|^2 \text{ for all } \mathbf{v} \in \mathbb{R}^p,$$

$$\text{such that } \|\mathbf{v}_{S^c}\|_1 \leq L \|\mathbf{v}_S\|_1$$

for some constant $L > 0$ and compatibility constant $\phi_0 > 0$ depending on S and L .

This assumption essentially means that the genuinely active predictors cannot be correlated too much. The condition is weaker than the restricted isometry condition (Candes and Tao, 2007). Like in the theory for the LASSO, we apply the condition with $L = 3$. In the Bayesian context for a spike-and-slab prior, Castillo et al. (2015) established the same rates under the condition with $L = 7$.

Assumption 3.3 (Bounded true mean condition). *The maximum of the absolute value of the expected response under the truth is bounded, that is, $\max_{1 \leq i \leq n} |\mathbb{E}_{\boldsymbol{\theta}^0}(Y_i)| = \mathcal{O}(1)$.*

It is reasonable to assume that the absolute expected value of the response under the truth is bounded for all sample points.

Assumption 3.4 (Non-collinearity condition). *When $p > n$, $\text{rank}(\mathbf{X}) = n$ and the singular values d_1, \dots, d_n of \mathbf{X} satisfy $\min\{d_j^2 : j = 1, \dots, n\} \gg na_n$.*

This assumption is made to tackle the $\mathbf{H}(a_n)$ matrix and ensures it does not behave very differently from the actual hat matrix.

Spike-and-slab or continuous shrinkage posterior may not need all the conditions our method needs for their convergence properties. This is analogous to the conditions needed for an ℓ_0 -penalized estimation versus its convex relaxation with the ℓ_1 -penalty giving rise to the LASSO. Spike-and-slab or its variants can be considered Bayesian

analogous of ℓ_0 -penalization methods, requiring exploring all possible models. There is a trade-off between exponential computing complexity versus a few additional restrictions. Moreover, the sparse projection-posterior can be justified by frequentist yardsticks, while most other Bayesian alternatives do not have similar justifications yet.

Theorem 3.1 (Estimation and prediction rate). *For $\lambda_n \asymp \sqrt{(\log p)/n}$, under Assumptions 3.1, 3.2, 3.3, 3.4 for every sequence $M_n \rightarrow \infty$, we have*

$$\Pi(\|\boldsymbol{\theta}^* - \boldsymbol{\theta}^0\|_1 \geq M_n s_0 \lambda_n | \mathbf{Y}) \rightarrow 0,$$

$$\Pi(n^{-1} \|\mathbf{X}(\boldsymbol{\theta}^* - \boldsymbol{\theta}^0)\|^2 \geq M_n s_0 \lambda_n^2 | \mathbf{Y}) \rightarrow 0$$

in probability under the true distribution.

Theorem 3.1 shows that when the tuning parameter used in the sparsity-inducing map is of the order $\sqrt{(\log p)/n}$, the posterior probabilities that the ℓ_1 -norm of the difference between the true parameter value and the sparse projections of the posterior samples will remain bounded above by $s_0 \lambda_n$ and that the Euclidean distance between the expected response under the true distribution and the corresponding predictor using the sparse projection-posterior is bounded by $s_0 \lambda_n^2$ converge in probability to 1 as the sample size grows indefinitely. This, in particular, implies posterior and prediction consistencies provided that $(\log p)/n \rightarrow 0$. The last condition restricts the growth of p relative to n , but only to nearly exponential in n , which will be assumed throughout the paper. For the spike-and-slab type priors, Castillo et al. (2015) derived comparable rates, but additionally assuming a revised compatibility condition (see Definition 2.2 and Definition 2.3 in Castillo et al. (2015)) under a setup they called the ‘sparse lambda regime’ for the choice of the prior.

3.1.2 Variable Selection Consistency

We show that the sparse projection-posterior is sign-consistent under a slightly stronger growth restriction on p relative to n , that is, $p = \mathcal{O}(e^{n^{b_3}})$ for some $b_3 < 1$. The strong irrerepresentable condition in Assumption 3.7 below helps avoid scenarios where zeros are matched, but opposite signs are used to estimate a model and allow recovery of support and signed signal magnitude. Given that the magnitude of the active predictors is bounded away from 0 by the threshold in Assumption 3.6 below, Theorem 3.2 below establishes that having observed the data, the sparse projection-posterior method consistently selects the true model and additionally matches the signs of the non-zero coefficients under the following assumptions.

Assumption 3.5 (Non-singularity condition). *The eigenvalues of the design matrix corresponding to the relevant covariates are bounded from below, that is, there exists a constant $M_2 > 0$ such that $\boldsymbol{\alpha}^\top (n^{-1} \mathbf{X}_{(1)}^\top \mathbf{X}_{(1)}) \boldsymbol{\alpha} \geq M_2$ for all $\|\boldsymbol{\alpha}\| = 1$.*

The assumption controls the behavior of the inverse of $\mathbf{C}_{n(11)}$. The correlation between variables can be controlled by restricting the eigenvalues of subsets of the design matrix to fall within a certain controlled interval.

Assumption 3.6 (Beta-min condition). *There exists $0 \leq b_1 < b_2 < 1$ and $M_3 > 0$ such that $s_0 = \mathcal{O}(n^{b_1})$ and $n^{(1-b_2)/2} \min_{1 \leq j \leq s_0} |\theta_j| \geq M_3$.*

This is a common assumption that bounds the number of active components, making sure that $s_0 < n$ holds (with much to spare), and additionally considers that the signal strengths of all the variables in the active set S_0 are larger than a specified value.

Assumption 3.7 (Strong Irrepresentable Condition). *There exists a vector of positive constants $\boldsymbol{\nu} = (\nu_1, \dots, \nu_{p-s_0})^\top$ such that $\max_{1 \leq j \leq p-s_0} |(\mathbf{C}_{n(21)} \mathbf{C}_{n(11)}^{-1} \text{sign}(\boldsymbol{\theta}_{(1)}^0))_j| \leq 1 - \nu_j$.*

A weaker version of this assumption simply replaces the positive fractional constant ν by 1, that is,

$$\max_{1 \leq j \leq p-s_0} |(\mathbf{C}_{n(21)} \mathbf{C}_{n(11)}^{-1} \text{sign}(\boldsymbol{\theta}_{(1)}^0))_j| < 1.$$

This assumption ensures that the total dependence of the noise variables on the signals cannot be larger than the irrepresentability constant (or 1 in the weak case). It restricts the extent to which the important predictors in the model can represent the irrelevant variables to facilitate proper distinction between noise and signal.

Theorem 3.2. *Let $\lambda_n \propto n^{(b_4-1)/2}$ and $p = \mathcal{O}(e^{n^{b_3}})$, where $0 \leq b_3 < b_4 < b_2 - b_1$. Then, under Assumptions 3.1, 3.5, 3.6, 3.7, we have that $\Pi(\{\text{sign}(\boldsymbol{\theta}) = \text{sign}(\boldsymbol{\theta}^0)\} | \mathbf{Y}) \rightarrow 1$ in probability under the true distribution.*

It will be seen that $\Pi(\{\text{sign}(\boldsymbol{\theta}) = \text{sign}(\boldsymbol{\theta}^0)\} | \mathbf{Y}) \geq \Pi(A_n \cap B_n | \mathbf{Y})$, where

$$A_n = \left\{ \left| \mathbf{C}_{n(11)}^{-1} \mathbf{Z}_{n(1)} \right| \leq \sqrt{n} (|\boldsymbol{\theta}_{(1)}^0| - \left| \frac{\lambda_n}{2n} \mathbf{C}_{n(11)}^{-1} \text{sign}(\boldsymbol{\theta}_{(1)}^0) \right|) \right\}, \quad (3.1)$$

$$B_n = \left\{ \left| \mathbf{C}_{n(21)} \mathbf{C}_{n(11)}^{-1} \mathbf{Z}_{n(1)} - \mathbf{Z}_{n(2)} \right| \leq \frac{\lambda_n}{2\sqrt{n}} \boldsymbol{\nu} \right\}. \quad (3.2)$$

The event A_n implies recovery of the signs of the true signals $\boldsymbol{\theta}_{(1)}^0$, and given A_n , the event B_n implies shrinking the coefficients of the irrelevant covariates to 0, that is, $\boldsymbol{\theta}_{(2)}^* = 0$. The sizes of these two events are traded off by the tuning parameter λ_n ; the lesser its value, the larger is A_n , and the smaller is B_n and vice versa. Bounding the $\Pi(A_n^c | \mathbf{Y})$ and $\Pi(B_n^c | \mathbf{Y})$ appropriately, the theorem can be established. A point to note here is that the penalty required to achieve this result is much stronger than the one needed for estimation or prediction consistency.

3.2 Uncertainty Quantification

3.2.1 Component-wise credible regions for $p \gg n$

To compute credible bands in a high-dimensional setting, we adopt a Bayesian version of the bias-correction technique introduced by [Zhang and Zhang \(2014\)](#) for the LASSO. This correction compensates for the LASSO's bias, albeit at the expense of sparsity. We apply a different immersion map, which includes this Bayesian bias-correction map, resulting in a non-sparse posterior distribution.

Let the LASSO-residuals $\mathbf{R}^{(j)}$ be obtained by regressing the j th column $\mathbf{X}^{(j)}$ of the design \mathbf{X} on the remaining columns, denoted by $\mathbf{X}^{(-j)}$, using the LASSO regularization. With $\lambda_j^{\mathbf{X}}$ standing for the tuning parameter, the LASSO of X_j on $\mathbf{X}^{(-j)}$ and the resulting residuals are respectively given by $\hat{\boldsymbol{\gamma}}^{(j)} = \arg \min_{\boldsymbol{\gamma} \in \mathbb{R}^{(p-1)}} \|\mathbf{X}^{(j)} - \mathbf{X}^{(-j)}\boldsymbol{\gamma}\|_2^2/n + \lambda_j^{\mathbf{X}} \|\boldsymbol{\gamma}\|_1$, and $\mathbf{R}^{(j)} = \mathbf{X}^{(j)} - \mathbf{X}^{(-j)}\hat{\boldsymbol{\gamma}}^{(j)}$. The tuning parameter $\lambda_j^{\mathbf{X}}$ may be chosen the same as the original LASSO tuning parameter λ_n . Unlike the least square residuals in low-dimension, the LASSO residuals are not orthogonal to $\mathbf{X}^{(-j)}$. In the present situation, [Zhang and Zhang \(2014\)](#) defined the j th component of the debiased estimator by $\hat{\theta}_j^{\text{DB}} = \mathbf{Y}^T \mathbf{R}^{(j)} / \mathbf{X}^{(j)T} \mathbf{R}^{(j)} = \hat{\theta}_j^{\text{L}} + (\mathbf{X}^{(j)T} \mathbf{R}^{(j)})^{-1} (\mathbf{Y} - \mathbf{X} \hat{\boldsymbol{\theta}}^{\text{L}})^T \mathbf{R}^{(j)}$, where $\hat{\boldsymbol{\theta}}^{\text{L}}$ is the LASSO estimator for $\boldsymbol{\theta}$. In high dimension ($p \gg n$), most subsets of n predictors will likely be linearly independent, and hence $\text{rank}(\mathbf{X}) = n$. If $\text{rank}(\mathbf{X}) = n$, $s_0 = o(\sqrt{n}/\log p)$, Assumptions [3.1](#), [3.2](#), [3.3](#), [3.4](#) hold and the tuning parameters $\lambda_n, \lambda_n^{\mathbf{X}}$ are both of the order of $\sqrt{(\log p)/n}$, then their estimator has an asymptotic normal distribution ([Zhang and Zhang, 2014](#)):

$$\hat{\sigma}^{-1} \frac{|\mathbf{X}^{(j)T} \mathbf{R}^{(j)}|}{\|\mathbf{R}^{(j)}\|} (\hat{\theta}_j^{\text{DB}} - \theta_j^0) \rightsquigarrow \mathcal{N}(0, 1), \quad (3.3)$$

for an estimator $\hat{\sigma}$ of σ , and consequently,

$$\lim_{n \rightarrow \infty} \mathbb{P}_{\boldsymbol{\theta}^0} \left(|\hat{\theta}_j^{\text{DB}} - \theta_j^0| < \Phi^{-1}(1 - \alpha/2) \frac{\hat{\sigma} \|\mathbf{R}^{(j)}\|}{|\mathbf{X}^{(j)T} \mathbf{R}^{(j)}|} \right) = 1 - \alpha$$

For uncertainty quantification, the form of the debiased LASSO estimator $\hat{\theta}_j^{\text{DB}}$ suggests using the immersion map $\iota^{\text{DB}} : \boldsymbol{\theta} \mapsto \boldsymbol{\theta}^{**}$ whose j th component θ_j^{**} is given by

$$\theta_j^* + \frac{\mathbf{R}^{(j)T} (\mathbf{X}\boldsymbol{\theta} - \mathbf{X}\boldsymbol{\theta}^*)}{\mathbf{R}^{(j)T} \mathbf{X}^{(j)}} = \frac{(\mathbf{X}\boldsymbol{\theta})^T \mathbf{R}^{(j)}}{\mathbf{X}^{(j)T} \mathbf{R}^{(j)}} - \sum_{k \neq j} P_{jk} \theta_k^*, \quad (3.4)$$

where $P_{jk} = \mathbf{X}^{(k)T} \mathbf{R}^{(j)} / \mathbf{X}^{(j)T} \mathbf{R}^{(j)}$, instead of the sparse-projection map used for estimation and variable selection. We shall call ι^{DB} the debiased sparse projection map and the corresponding induced distribution the debiased sparse projection-posterior

distribution. In the following results, we show a type of the Bernstein-von Mises theorem that the debiased sparse projection-posterior distribution of $\sqrt{n}(\theta_j^{**} - \theta_j^0)$ can be approximated by a normal distribution with the mean given by the normalized debiased LASSO estimator of Zhang and Zhang (2014) and the variance asymptotically equivalent to the asymptotic variance of the debiased LASSO estimator. Consequently, the asymptotic frequentist coverage of a credible ball for θ_j^{**} will agree with the corresponding credibility for all $j \in \{1, 2, \dots, p\}$. The property extends immediately to any fixed-dimensional linear function of $\boldsymbol{\theta}$.

Theorem 3.3 (Bernstein-von Mises Theorem). *If Assumptions 3.1, 3.2, 3.3, 3.4 hold and $s_0 = o(\sqrt{n}/\log p)$ and $\text{rank}(\mathbf{X}) = n$, then*

$$\max_{1 \leq j \leq p} \sup_B \left| \Pi(\sqrt{n}(\theta_j^{**} - \theta_j^0) \in B | \mathbf{Y}) - \mathcal{N}_p(B; m_j, \Sigma_{jj}) \right| \rightarrow 0,$$

where

$$m_j = \sqrt{n} \left(\frac{\mathbf{R}^{(j)\top} \mathbf{X} \hat{\boldsymbol{\theta}}^R}{\mathbf{R}^{(j)\top} \mathbf{X}^{(j)}} - \sum_{k=1}^p P_{jk} \theta_k^0 \right), \quad (3.5)$$

$$\Sigma_{jj} = n \sigma_0^2 \left(\frac{\mathbf{R}^{(j)\top} \mathbf{H}(a_n) \mathbf{R}^{(j)}}{|\mathbf{X}^{(j)\top} \mathbf{R}^{(j)}|^2} \right). \quad (3.6)$$

Define $C_j = [\tilde{\theta}_j - q_{j,\alpha}, \tilde{\theta}_j + q_{j,\alpha}]$ to be the symmetric $(1 - \alpha)$ -credible interval for θ_j , $j = 1, \dots, p$, where $\tilde{\theta}_j$ is the median of the posterior distribution of θ_j^{**} and $q_{j,\alpha}$ is the $(1 - \alpha/2)$ -quantile of the posterior distribution of $|\theta_j^{**} - \tilde{\theta}_j|$. The following result shows that these can be regarded as approximate $(1 - \alpha)$ -confidence intervals.

Corollary 3.3.1. *(Coverage of credible interval for θ_j) Under Assumptions 3.1, 3.2, 3.3, 3.4,*

$$\mathbb{P}_{\theta^0}(\theta_j^0 \in C_j) \rightarrow 1 - \alpha \text{ uniformly for all } j = 1, 2, \dots, p.$$

From the proof, it will also follow that the conclusion holds for the equal-tailed $(1 - \alpha)$ -credible interval $C_j = [l_j, u_j]$ for θ_j , $j = 1, \dots, p$, where $\Pi(\theta_j^{**} < l_j) = \alpha/2$ and $\Pi(\theta_j^{**} > u_j) = \alpha/2$.

3.2.2 Credible ellipsoid

Joint credible sets for the relevant predictors in the model automatically address any interrelationships between the coefficients of interest. When individual component-wise credible intervals are provided, these are ignored. We construct a sparse, credible ellipsoid for $\boldsymbol{\theta}$ in this subsection.

Let the model formed by the true active variables be denoted by $F_n = \{\boldsymbol{\theta}^* : \text{sign}(\boldsymbol{\theta}^*) = \text{sign}(\boldsymbol{\theta}^0)\}$. We know from Theorem 3.2 that the true model is selected

with probability tending to one when the sample size goes to infinity, that is, $\Pi(\boldsymbol{\theta}^* \in F_n | \mathbf{Y}) \rightarrow 1$ in probability under the true distribution. Thus, theoretically, we can identify the set F_n from posterior sampling with large sample sizes. Conditioned on $\boldsymbol{\theta}^* \in F_n$, the probability of any event, say A , satisfies

$$\mathbb{P}(A|F_n) = \frac{\mathbb{P}(A \cap F_n)}{\mathbb{P}(F_n)} \rightarrow \mathbb{P}(A).$$

Using this idea, we can now concentrate only on the coverage properties of the covariates selected by the projection method with high probability (tending to 1). Without loss of generality, the set of selected active predictors is $\{1, \dots, s_0\}$ and so $\mathbf{X}_{(1)} \in \mathbb{R}^{n \times s_0}$ is the matrix containing only the important predictors for all n samples.

Let \hat{S} stand for the highest maximum sparse projection posterior probability model. Restricted to the selected model \hat{S} , let $\boldsymbol{\theta}_{\hat{S}}^{\text{PS}}$ stand for the vector of components of $\boldsymbol{\theta}$ in \hat{S} only. Then the conditional posterior distribution of $\boldsymbol{\theta}_{\hat{S}}^{\text{PS}}$ given σ based on only the selected predictors \hat{S} is $\mathcal{N}_{\hat{s}}(\hat{\boldsymbol{\theta}}_{\hat{S}}^{\text{R,PS}}, \sigma^2(\mathbf{X}_{\hat{S}}^{\text{T}}\mathbf{X}_{\hat{S}} + a_n\mathbf{I}_{\hat{s}})^{-1})$, where $\hat{\boldsymbol{\theta}}_{\hat{S}}^{\text{R,PS}} = (\mathbf{X}_{\hat{S}}^{\text{T}}\mathbf{X}_{\hat{S}} + a_n\mathbf{I}_{\hat{s}})^{-1}\mathbf{X}_{\hat{S}}^{\text{T}}\mathbf{Y}$, the post-selection ridge regression estimator based on the selected predictors \hat{S} and \hat{s} is the cardinality of \hat{S} . For a given credibility level $1 - \alpha$, define the post-selection credible ellipsoid $D_{n,1-\alpha}^{\text{PS}}$ to be

$$\left\{ \begin{pmatrix} \boldsymbol{\theta}_{\hat{S}} \\ \mathbf{0}_{\hat{S}^c} \end{pmatrix} : (\boldsymbol{\theta}_{\hat{S}} - \hat{\boldsymbol{\theta}}_{\hat{S}}^{\text{R,PS}})^{\text{T}}(\mathbf{X}_{\hat{S}}^{\text{T}}\mathbf{X}_{\hat{S}} + a_n\mathbf{I}_{\hat{s}})(\boldsymbol{\theta}_{\hat{S}} - \hat{\boldsymbol{\theta}}_{\hat{S}}^{\text{R,PS}}) \leq r_{\alpha}\sigma^2 \right\},$$

where the size r_{α} is chosen such that $\Pi(\boldsymbol{\theta} \in D_{n,1-\alpha}^{\text{PS}} | \mathbf{Y}) = 1 - \alpha$. We claim that $D_{n,1-\alpha}^{\text{PS}}$ also serves as an asymptotic $(1 - \alpha)$ -confidence region. Informally, this holds because by Theorem 3.2, $\hat{S} = S_0$ with probability tending to one, provided the conditions of the theorem are satisfied so that the setup effectively reduces to that of the Bernstein-von Mises theorem with a fixed set of parameters. More elaborately, the posterior is essentially the one based on the correct set of predictors S_0 with mean the ridge regression estimator based on predictors in S_0 , and dispersion matrix approximately $\sigma_0^2 n^{-1} \mathbf{C}_{(11)}$. By Lemma 10.6, the ridge regression estimator is asymptotically normal centered at $\boldsymbol{\theta}_{S_0}^0$ and dispersion matrix $\sigma_0^2 n^{-1} \mathbf{C}_{(11)}$. The approximate Bayes-frequentist agreement leads to the correct asymptotic coverage. The discussion is formalized in the next theorem.

Theorem 3.4. *Let S_0 be fixed, and Assumptions 3.1, 3.4, 3.5, 3.6 and 3.7 hold. Let r_{α} stand for the posterior $(1 - \alpha)$ -quantile of $(\boldsymbol{\theta}_{\hat{S}}^{\text{PS}} - \hat{\boldsymbol{\theta}}_{\hat{S}}^{\text{R,PS}})^{\text{T}}(\mathbf{X}_{\hat{S}}^{\text{T}}\mathbf{X}_{\hat{S}} + a_n\mathbf{I}_{\hat{s}})(\boldsymbol{\theta}_{\hat{S}}^{\text{PS}} - \hat{\boldsymbol{\theta}}_{\hat{S}}^{\text{R,PS}})$. Then the coverage $\mathbb{P}_{\boldsymbol{\theta}^0}(\boldsymbol{\theta}^0 \in D_n) \rightarrow 1 - \alpha$, where D_n is*

$$\{\boldsymbol{\theta}_{\hat{S}} : (\boldsymbol{\theta}_{\hat{S}} - \hat{\boldsymbol{\theta}}_{\hat{S}}^{\text{R,PS}})^{\text{T}}(\mathbf{X}_{\hat{S}}^{\text{T}}\mathbf{X}_{\hat{S}} + a_n\mathbf{I}_{\hat{s}})(\boldsymbol{\theta}_{\hat{S}} - \hat{\boldsymbol{\theta}}_{\hat{S}}^{\text{R,PS}}) \leq r_{\alpha}\} \times \{\mathbf{0}_{\hat{S}^c}\}.$$

Oftentimes, $\Pi(F_n|\mathbf{Y})$ may not be close to 1 unless the sample size is impractically large since the number of possible models is exceptionally high. However, the only requirement is that the correct model F_n has the highest posterior probability. This happens more commonly — $\Pi(F_n|\mathbf{Y}) > 1/2$ gives a sufficient condition.

3.3 Tuning

As seen above, recovery and prediction accuracy both require the tuning parameter $\lambda_n \asymp \sqrt{(\log p)/n}$, whereas correct model selection is guaranteed when $\lambda_n \propto n^{(b_4-1)/2}$ with some $b_3 \leq b_4 < b_2 - b_1$. As discussed earlier, different λ_n can be chosen for different purposes, giving different immersion posterior for different inferential problems. Typically, slightly larger values of λ_n will give accurate model selection. The asymptotic theory guides the choice, but a data-driven choice of the tuning parameter is desirable from practical considerations. One way to regularize the model for optimal estimation and prediction could be to fit the model using the lasso with a wide range of values of λ_n and choose that which gives the lowest prediction error. This is justified because the requirement on the tuning parameter λ_n for prediction consistency is the same as the LASSO. Since accurate model selection requires a larger penalty, depending on how much larger the prediction error could be allowed, we may keep increasing the value of the tuning parameter until an anticipated level of sparsity is achieved. This should induce greater sparsity in the posterior distribution while keeping the prediction error within a tolerable limit.

3.4 Error variance

As the sparse projection-posterior approach uses conditional draws given σ^2 , the posterior distribution of σ must be consistent to ensure the asymptotic frequentist properties of the sparse projection-posterior. However, unless p is of a smaller order of n , the marginal vanilla posterior for σ^2 obtained from the regression model using a standard prior is inconsistent. Putting the non-informative prior $\text{Gamma}(0,0)$ on the precision parameter $\tau = \sigma^{-2}$ so that the prior density is $p(\tau) = 1/\tau$, we obtain the $\text{Gamma}(n/2, n\hat{\sigma}_n^2/2)$ posterior for τ , where $\hat{\sigma}_n^2 = n^{-1}\mathbf{Y}^T(\mathbf{I}_n - \mathbf{H}(a_n))\mathbf{Y}$. Note that the posterior mean $\mathbb{E}(\tau|\mathbf{Y}) = n/(\mathbf{Y}^T(\mathbf{I}_n - \mathbf{H}(a_n))\mathbf{Y})$ blows up as n grows (cf., Lemma 10.2). This is analogous to the inconsistency of standard estimators like the maximum likelihood estimator or the unbiased variance estimator. The technique of immersion posterior can be used to rectify the problem. This can be corrected by applying a data-dependent immersion map to τ . For a data-dependent factor κ , consider the map $\tau \mapsto \kappa\tau$. Its induced posterior distribution is thus given by $(\kappa\tau|\mathbf{Y}) \sim \text{Gamma}(n/2, \kappa^{-1}n\hat{\sigma}_n^2/2)$, which has expectation $\kappa/\hat{\sigma}_n^2$. If we choose

$\kappa = \hat{\sigma}_n^2/\tilde{\sigma}^2$, where $\tilde{\sigma}^2$ is a consistent estimator of σ^2 such as in Sun and Zhang (2012), then the posterior mean of the immersion posterior corresponding to the immersion map $\tau \mapsto \kappa\tau$ is a consistent point estimator for $\tau = \sigma^{-2}$. The posterior variance of $\kappa\tau$ is given by $2\kappa^2/(n\hat{\sigma}_n^4) = 2/(n\tilde{\sigma}^4)$, which goes to zero as $n \rightarrow \infty$ since $\tilde{\sigma}^2$ converges to the finite positive constant σ_0^2 by the consistency of $\tilde{\sigma}^2$ for σ^2 . Thus, the immersion posterior for τ using the data-dependent immersion map $\tau \mapsto \kappa\tau$ is consistent by Chebyshev's inequality. As the correspondence between τ and σ is smooth and one-to-one, the induced immersion posterior for σ is also consistent. In other words, we use the immersion map $\sigma \mapsto \sigma^* = (\tilde{\sigma}/\hat{\sigma}_n)\sigma$ for σ , and the joint immersion map for $(\boldsymbol{\theta}, \sigma)$ is given by $(\boldsymbol{\theta}, \sigma) \mapsto (\boldsymbol{\theta}^*, (\tilde{\sigma}/\hat{\sigma}_n)\sigma)$ in place of their original posterior distributions. To sample from the joint immersion posterior, we sample τ from $\text{Gamma}(n/2, n\tilde{\sigma}^2/2)$, compute $\sigma = \tau^{-1/2}$, set $\sigma^* = (\tilde{\sigma}/\hat{\sigma}_n)\sigma$, draw $\boldsymbol{\theta}$ from $\mathcal{N}_n(\hat{\boldsymbol{\theta}}^R, \sigma^{*2}(\mathbf{X}^T\mathbf{X} + a_n\mathbf{I}_p)^{-1})$ and compute $\boldsymbol{\theta}^*$ from (2.4) for the appropriate choice of λ_n depending on the purpose such as estimation, variable selection or uncertainty quantification. Consequently, we can find a shrinking neighbourhood \mathcal{U}_n of σ_0 such that $\Pi(\sigma^* \in \mathcal{U}_n|\mathbf{Y}) \rightarrow 1$ in probability as $n \rightarrow \infty$.

4 Numerical Results

We consider the linear regression model with response $\mathbf{Y} \in \mathbb{R}^p$ and fixed design $\mathbf{X} \in \mathbb{R}^{n \times p}$, and its rows are sampled from $\mathcal{N}_p(\mathbf{0}, \boldsymbol{\Sigma})$. For the Bayesian method, we use the median probability model (MPM) (Barbieri and Berger, 2004), which chooses those variables in the final model whose marginal posterior probability of being included is at least 0.5 to select predictors. We use an estimator with zeroes at all components not selected in more than 50% MCMC iterations. The estimator takes the average of all the R samples for the remaining components, where R is the number of MCMC draws. A comparison between Bayesian and frequentist methods included in the study of estimation accuracy is based on the $\text{MSE} = (\hat{\boldsymbol{\theta}} - \boldsymbol{\theta}^0)^T \boldsymbol{\Sigma} (\hat{\boldsymbol{\theta}} - \boldsymbol{\theta}^0)$. For a variable selection procedure, we define True Positives (TP) as the signals correctly identified to be non-null, False Positives (FP) as the noise variables falsely selected as active variables, True Negatives (TN) as the null variables correctly not selected by the model and finally False Negatives (FN) as the signals mistakenly left out of the model. To compare different variable selection methods, we report three quantities, namely, True Positive Rate (TPR) which is the ratio of correctly selected predictors to the total number of true signals (s_0), $\text{TPR} = \text{TP}/(\text{TP} + \text{FN})$, False Discovery Proportion (FDP) which is the ratio of falsely selected predictors to the number of selected signals, $\text{FDP} =$

FP/(FP+TP) and Matthew’s correlation coefficient (MCC):

$$\text{MCC} = \frac{\text{TN} \times \text{TP} - \text{FN} \times \text{FP}}{\sqrt{(\text{TP} + \text{FP})(\text{TP} + \text{FN})(\text{TN} + \text{FP})(\text{TN} + \text{FN})}}.$$

The closer the MCC value is to 1, the better its selection ability. For uncertainty quantification, we report the mean coverage and length of 95% confidence/credible intervals for the s_0 active covariate coefficients and again for the $p - s_0$ noise, averaged over the number of replications (M), which is taken to be 100 unless mentioned otherwise. For Bayesian methods, credible regions are constructed using sample quantile values from posterior draws. The estimation accuracy, model selection ability, and coverage performance of the projection-posterior are compared with those of the Bayesian LASSO (BLASSO), spike-and-slab LASSO (SSLASSO), posterior from the horseshoe prior, minimax-concave penalty (MCP) estimator, LASSO, debiased LASSO, and bootstrap LASSO. The last two are the only frequentist methods included in the study of confidence intervals. The competing Bayesian methods are computed based on $R = 10000$ MCMC runs to provide results comparable to frequentist methods. A burn-in of 2000 samples is administered before collecting posterior draws. We introduce and use the R package named `sparseProj` (Pal, 2024) to implement the sparse projection-posterior method.

4.1 Simulation Study 1

4.1.1 Simulation Setup

We consider three cases for the simulation study. In the first case, we compare the model selection and estimation performances of different Bayesian and frequentist procedures in a sparse linear regression setup, where we assume p grows like $n^{2/3}$, e.g., $n = 1000$, $p = 100$, and the number of active predictors $s_0 = 10$. The second case explores the scenario when n and p are similar, e.g., $n = p = 300$ and $s_0 = 10$. Lastly, in the third case, we allow p to grow exponentially with n like e^{n^c} for some $0 < c < 1$. We choose $n = 100$ and $c = 0.45$ so that $p = 2000$ and set s_0 to 10. Here, two scenarios are explored: one where the design \mathbf{X} consists of all independent covariates ($\Sigma = \sigma^2 \mathbf{I}$, $\sigma^2 = 1$ where \mathbf{I} is the $p \times p$ identity matrix), and the other considers an autoregressive correlation structure which assumes that the correlation between variables gradually decreases as the distance between their relative positions increases ($\Sigma = ((\sigma_{ij}))$, $\sigma_{ij} = \rho^{|j-i|}$, where $\rho = 0.7$). The coefficient vector $\boldsymbol{\theta}$ is set up such that the first $s_0 = 10$ components correspond to moderately strong signals, that is, $\theta_j = 2$ for $j = 1, \dots, s_0$, and the remaining $p - s_0$ components are zeroes. The Bayesian LASSO has been skipped in the last two cases due to its exceptionally long

run times.

4.1.2 Tuning parameters

The tuning parameters in LASSO and MCP are all computed by a 10-fold cross-validation. The cross-validated LASSO tuning value is used as an empirical Bayes estimate of the common parameter λ in the prior distributions of the local shrinkage parameters. The target acceptance rate in the SSVS method is set to 0.345. All other parameters in any model used are set to their defaults. For our method, the posterior draws of $\boldsymbol{\theta}$ from the multivariate Gaussian have been shrunk to $\boldsymbol{\theta}^*$ using the projection map with the regularization parameter same as the one chosen by CV in LASSO as the two methods share all theoretical properties.

4.1.3 Simulation Results

We investigated the time taken for one run of each method in this study for both small- p and large- p cases. In Table 1 reported are the mean times (in seconds) to finish $R = 10000$ MCMC runs of each of the Bayesian methods along with one run of the debiased LASSO and the bootstrap LASSO with 5000 replicates. The projection method and the bootstrap LASSO have similar computing costs. Computation times under $p = 2000$ for SSVS and BLASSO are excessive (in hours) and have not been reported along with the other faster computing methods.

We see in Figure 1 that the MSEs in the low-dimensional model with $n = 1000 > p = 100$ are much smaller than the ones from the high-dimensional model with $p = 2000 > n = 100$ for all the methods and for both design types. Performance-wise, in the low-dimensional setting, the LASSO has the largest estimation error, but other methods have very comparable performance. The Bayesian LASSO was skipped in the high-dimensional setting due to its high computing time. The LASSO and the sparse projection-posterior mean have somewhat higher MSE than other methods for independent predictors, but the difference is minimal for correlated predictors. In all cases, the MCP, horseshoe, SSVS, and SSLASSO generally have similar average estimation errors.

In Table 2, we report the measures for variable selection corresponding to both the small- p ($n = 1000, p = 100$) and large- p ($n = 100, p = 2000$) regimes and both design types. The SSVS maintained its best selection performance in low- and high-dimensional cases, followed by the SSLASSO and the projection method. However, the SSLASSO fails to maintain its consistency under correlated predictors, whereas the projection-posterior method is hardly affected by it. When $p < n$, the Bayesian LASSO selects many noise variables, causing its FDP to be the highest and, consequently, its MCC to be the lowest. The MCP does a good job of identifying the correct signals.

Model	Debiased LASSO	Bootstrap LASSO	Horseshoe	SSLASSO	SSVS	Bayesian LASSO	Projection
$n = 1000, p = 100$	20.5 (2.39)	17.2 (2.73)	25.7 (4.01)	<1 (0.00)	267.8 (1.61)	227.4 (15.38)	17.8 (2.14)
$n = 100, p = 2000$	339.533 (22.87)	116.1 (11.03)	234.7 (16.21)	18.468 (3.59)	-	-	121.0 (12.09)

Table 1: The mean (sd) time (in seconds) to complete one run of the competing methods, averaged over M replications.

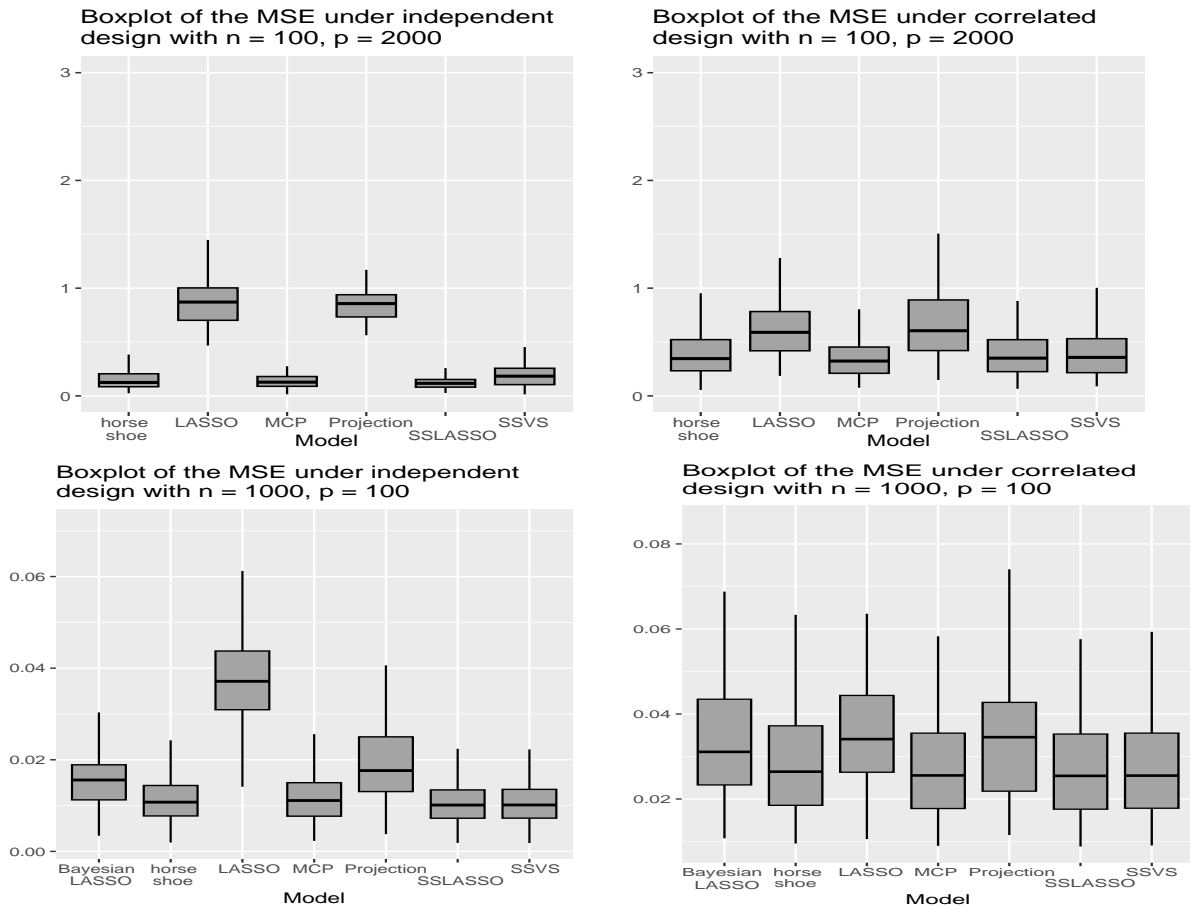


Figure 1: Boxplots of the $n \times \text{MSE}$ s for different methods averaged over $M = 100$ replications corresponding to the different cases are provided starting from large- p independent and correlated design, followed by the same for small- p .

The same conclusion can be made from the plots in the third and fourth panels of Figure 2, which show the boxplots of the MCC values of the competing methods. On average, the sparse projection-posterior-based method is comparable to the horseshoe method but performs better when the design matrix has an underlying correlation structure. Overall, from this limited simulation study, it can be concluded that the method proposed here has good selection properties. In addition, as will be shown next, the method can provide coverage for the signals, but the SSVS and SSLASSO fail to do so.

We compare the coverage of 95% confidence or credible regions from the different

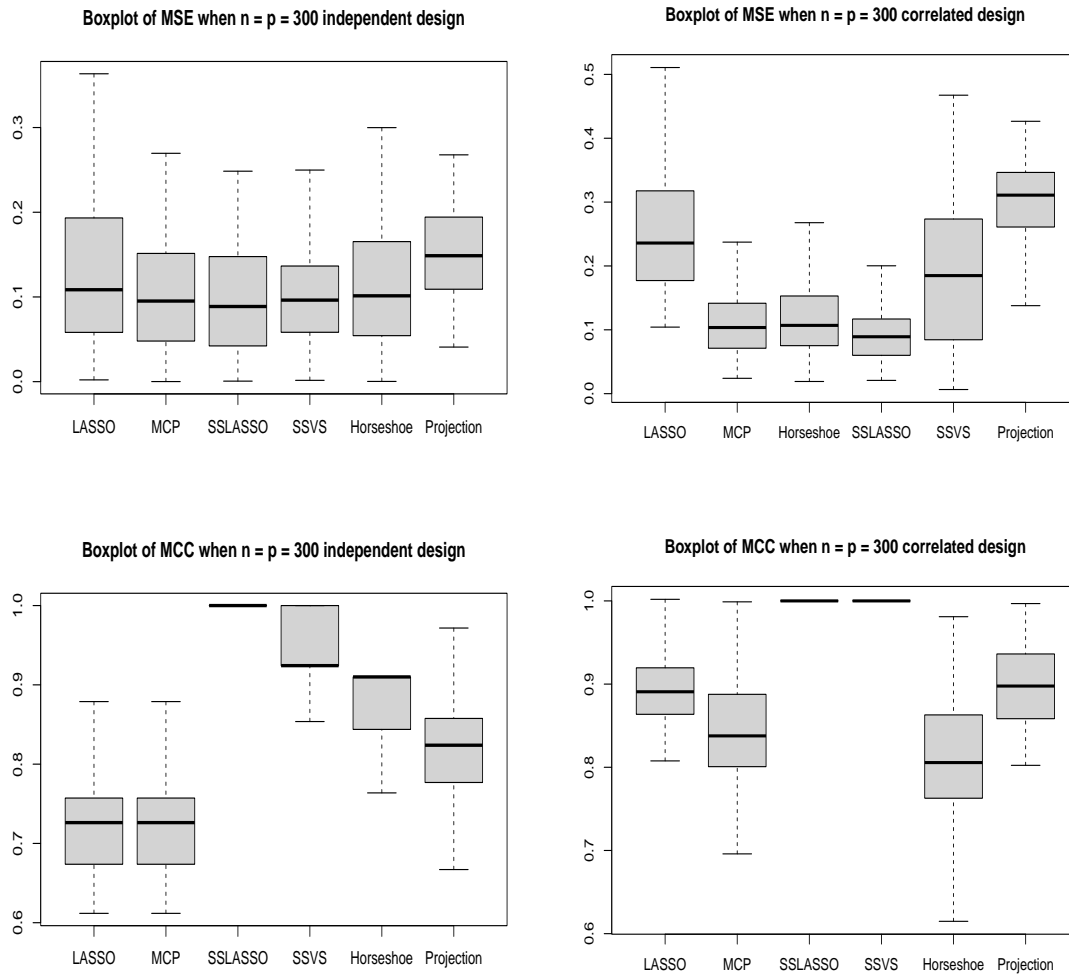


Figure 2: The boxplots of the $n \times \text{MSE}$ s of all the comparing methods are provided for the independent design (first) and the correlated design (second). The boxplots of the MCC values of all the methods are provided for the independent design (third) and the correlated design (fourth). All the plots correspond to $n = p = 300$ and $M = 100$ replications.

(n, p, s_0)	Methods	Uncorrelated Design			Correlated Design		
		TPR	FDP	MCC	TPR	FDP	MCC
$n = 100$ $p = 2000$ $s_0 = 10$	LASSO	1	0.154 (0.183)	0.913 (0.114)	1	0.145 (0.017)	0.918 (0.105)
	MCP	1	0.056 (0.125)	0.958 (0.072)	1	0.056 (0.015)	0.969 (0.065)
	Horseshoe	1	0.013 (0.047)	0.990 (0.025)	1	0.015 (0.047)	0.992 (0.025)
	SSVS	1	0	1	1	0	1
	SSLASSO	1	0	1	0.995 (0.001)	0.005 (0.050)	0.995 (0.046)
	Projection	1	0.084 (0.063)	0.944 (0.108)	1	0.018 (0.037)	0.991 (0.019)
$n = 1000$ $p = 100$ $s_0 = 10$	LASSO	1	0.140 (0.013)	0.935 (0.081)	1	0.129 (0.012)	0.979 (0.019)
	MCP	1	0.125 (0.013)	0.964 (0.017)	1	0.108 (0.011)	0.996 (0.084)
	Horseshoe	1	0.006 (0.023)	0.986 (0.013)	1	0.004 (0.034)	0.991 (0.007)
	BLASSO	1	0.292 (0.104)	0.819 (0.070)	1	0.269 (0.101)	0.833 (0.089)
	SSVS	1	0	1	1	0	1
	SSLASSO	1	0	1	1	0.001 (0.000)	0.999 (0.005)
Projection	1	0.015 (0.038)	0.991 (0.022)	1	0.052 (0.042)	0.984 (0.030)	

Table 2: Variable selection performances of the different methods corresponding to the small- p and large- p cases. The mean (sd) of $M = 100$ replications are reported.

methods included in the simulation. In Tables 3 and 4, we report the mean coverage averaged over the M replicates corresponding to the uncorrelated and correlated designs respectively, but separately for active and inactive variables. In general, coverage and length-wise, all methods do better when the variables are independent. On the Bayesian side, only the proposed sparse projection-posterior method reaches close to the desired coverage. The average lengths of all the intervals increase significantly to provide the same extent of coverage when the dimension p grows with the sample size n . The existing Bayesian methods provide coverage if the parameter is zero but fail to attain 95% coverage for non-zero parameter values corresponding to active predictors. Also, the average coverage of signals deteriorates in the correlated design setting. However, when $p \gg n$, the only Bayesian method that provides good coverage of the signals is the sparse projection-posterior method. The plots in Figure 3 show the coverage and length of credible/confidence regions averaged over all the signal variables for all competing methods. For small- p and $n = p$ cases, the sparse projection posterior method attains desirable coverage with a very small length, making it the best candidate. Its performance degrades when the dimension exceeds n but is still better than most methods.

In Figure 4, we present individual coverage and interval lengths for two randomly selected signals and two randomly selected noise components in all four settings. These settings compare intervals produced by the horseshoe, sparse projection-posterior, de-biased LASSO (ZnZ), and bootstrap LASSO for active (1 and 6) and noise (50 and 100) variables. Both signals have a true coefficient of 2. The plots show frequentist methods, and the Bayesian sparse posterior-projection method offers good coverage and comparable interval lengths. The horseshoe prior, in particular, exhibits slightly shorter lengths, especially for noise variables, consistent with results in Table 3. Im-

(n, p, s_0)	Methods	Uncorrelated Design			
		Signal Coverage	Length of Intervals for Signals	Noise Coverage	Length of Intervals for Noise
$n = 100$ $p = 2000$ $s_0 = 10$	Bootstrap LASSO	0.908 (0.025)	0.275 (0.099)	0.984 (0.005)	0.574 (0.002)
	ZnZ	0.949 (0.019)	0.525 (0.101)	0.947 (0.005)	0.527 (0.010)
	Debiased LASSO	0.910 (0.091)	0.475 (0.095)	0.943 (0.005)	0.463 (0.009)
	Horseshoe	0.819 (0.026)	0.146 (0.031)	0.979 (0.003)	0.442 (0.002)
	Projection	0.908 (0.094)	0.453 (0.023)	0.967 (0.004)	0.427 (0.003)
$n = p = 300$ $s_0 = 10$	Bootstrap LASSO	0.931 (0.082)	0.259 (0.022)	0.972 (0.019)	0.372 (0.011)
	ZnZ	0.958 (0.071)	0.335 (0.240)	0.952 (0.011)	0.355 (0.091)
	Debiased LASSO	0.951 (0.073)	0.380 (0.375)	0.949 (0.016)	0.360 (0.108)
	SSVS	0.870 (0.131)	0.098 (0.014)	0.999 (0.000)	0.163 (0.032)
	Horseshoe	0.891 (0.099)	0.102 (0.015)	0.999 (0.000)	0.205 (0.005)
$n = 1000$ $p = 100$ $s_0 = 10$	Projection	0.945 (0.011)	0.159 (0.006)	0.977 (0.001)	0.267 (0.015)
	Bootstrap LASSO	0.929 (0.080)	0.122 (0.003)	0.945 (0.024)	0.046 (0.009)
	ZnZ	0.954 (0.076)	0.134 (0.003)	0.948 (0.022)	0.133 (0.003)
	Debiased LASSO	0.950 (0.082)	0.127 (0.003)	0.945 (0.023)	0.126 (0.003)
	Horseshoe	0.857 (0.108)	0.099 (0.002)	0.991 (0.012)	0.052 (0.003)
	BLASSO	0.835 (0.115)	0.100 (0.002)	0.999 (0.003)	0.018 (0.004)
	SSVS	0.841 (0.112)	0.099 (0.002)	0.998 (0.000)	0.038 (0.001)
	Projection	0.966 (0.111)	0.103 (0.003)	0.949 (0.030)	0.088 (0.002)

Table 3: The average (standard error) coverage and average (standard error) length of the signals (columns 1 and 2) and noise variables (columns 3 and 4) corresponding to $p > n$ (Upper), $p = n$ (Middle) and $p < n$ (Lower) for the independent design respectively.

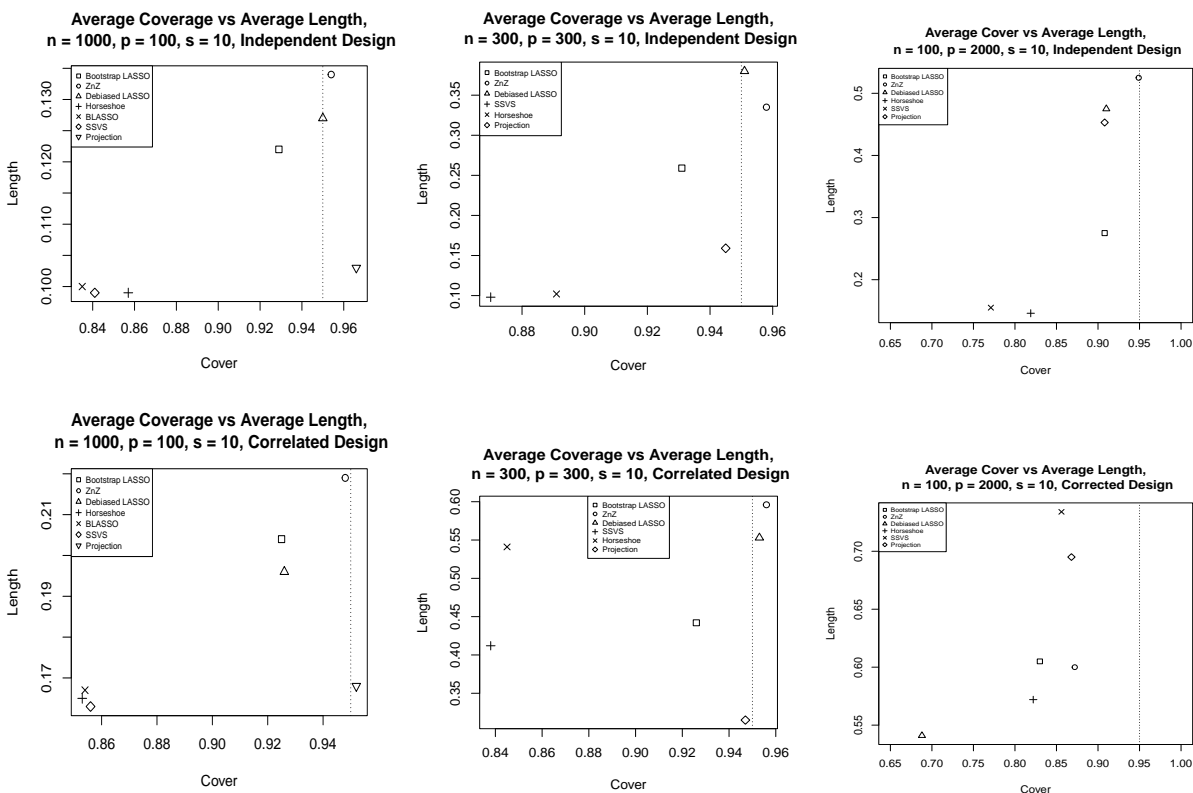


Figure 3: The average coverage probabilities for the 10 signals are plotted against the average lengths of the confidence/credible intervals for the competing methods.

(n, p, s_0)	Methods	Correlated Design			
		Signal Coverage	Length of Intervals for Signals	Noise Coverage	Length of Intervals for Noise
$n = 100$ $p = 2000$ $s_0 = 10$	Bootstrap LASSO	0.830 (0.180)	0.605 (0.139)	0.992 (0.004)	0.523 (0.002)
	ZnZ	0.872 (0.146)	0.600 (0.081)	0.951 (0.006)	0.586 (0.007)
	Debiased LASSO	0.688 (0.147)	0.541 (0.063)	0.949 (0.004)	0.564 (0.005)
	Horseshoe	0.822 (0.155)	0.572 (0.067)	0.966 (0.002)	0.359 (0.007)
	SSVS	0.856 (0.122)	0.734 (0.226)	0.972 (0.001)	0.312 (0.015)
	Projection	0.868 (0.131)	0.695 (0.011)	0.982 (0.002)	0.548 (0.007)
$n = p = 300$ $s_0 = 10$	Bootstrap LASSO	0.926 (0.090)	0.442 (0.031)	0.966 (0.022)	0.288 (0.009)
	ZnZ	0.956 (0.067)	0.596 (0.212)	0.947 (0.010)	0.352 (0.077)
	Debiased LASSO	0.953 (0.067)	0.553 (0.478)	0.948 (0.014)	0.320 (0.091)
	SSVS	0.838 (0.119)	0.412 (0.103)	0.998 (0.001)	0.120 (0.150)
	Horseshoe	0.845 (0.107)	0.541 (0.029)	0.996 (0.001)	0.361 (0.007)
	Projection	0.947 (0.013)	0.315 (0.010)	0.968 (0.007)	0.464 (0.007)
$n = 1000$ $p = 100$ $s_0 = 10$	Bootstrap LASSO	0.925 (0.072)	0.204 (0.005)	0.953 (0.029)	0.119 (0.015)
	ZnZ	0.948 (0.070)	0.219 (0.005)	0.953 (0.025)	0.221 (0.004)
	Debiased LASSO	0.926 (0.088)	0.196 (0.005)	0.952 (0.023)	0.198 (0.004)
	Horseshoe	0.853 (0.102)	0.165 (0.003)	0.979 (0.006)	0.061 (0.005)
	BLASSO	0.854 (0.106)	0.167 (0.004)	0.982 (0.002)	0.022 (0.007)
	SSVS	0.856 (0.099)	0.163 (0.003)	0.991 (0.002)	0.045 (0.003)
	Projection	0.952 (0.101)	0.168 (0.002)	0.969 (0.019)	0.092 (0.008)

Table 4: The average (standard error) coverage and average (standard error) length of the signals (columns 1 and 2) and noise variables (columns 3 and 4) corresponding to $p > n$ (Upper), $p = n$ (Middle) and $p < n$ (Lower) for the correlated design respectively.

portantly, our proposed method consistently covers the true signal.

We also verify the coverage of the credible ellipsoid introduced in Section 3.2.2 for the three cases studied in this section, namely $n = 1000, p = 100$, $n = p = 300$ and finally $n = 100, p = 1000$. The reported results are the mean coverage values over $M = 100$ repetitions. For the low-dimensional case, the average coverage of the credible ellipsoid for the signals is 0.954 with standard error of 0.004. When sample size and dimension are both equal to 300, the average coverage and standard error are respectively 0.951 and 0.008. Finally, in the higher dimensional setting, we observe the average coverage by the ellipsoid to be 0.947 with a standard error of 0.010.

4.2 Simulation Study 2: Distributed Computing and Credible Ellipsoid

This section shows the usefulness of the sparse projection-posterior method when the sample size is too huge. Besides the ability of our proposed method to accommodate distributed computing, the scope to jointly quantify for the signal uncertainty helps avoid the debiasing map. Since debiasing is computationally heavy, bypassing it gives even more computational edge over and above the distributed computation when n is very large. We will conduct the following simulation to verify this claim. Here, we generate the design matrix from the normal distribution with $n = 100000$ rows and $p = 500$ columns. We set the sparsity to $s_0 = 20$ and generate the signals from the Uniform(1,3) distribution. We randomly divide the data into 100 splits to contain

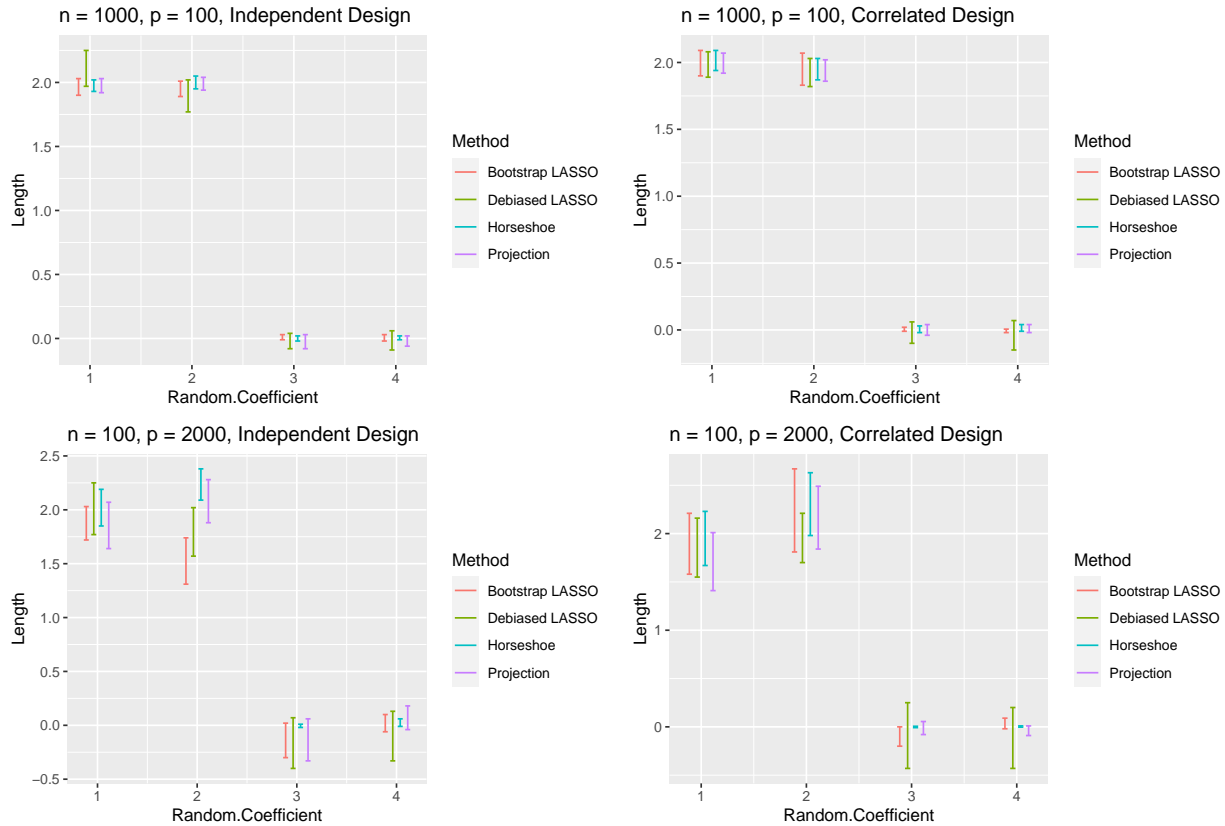


Figure 4: Plots of the randomly selected signal and noise coefficients for different methods corresponding to the independent design ($p > n$: lower left panel) and the correlated design ($p > n$: lower right panel) and similarly, the independent design ($p < n$: upper right panel) and the correlated design ($p < n$: upper left panel).

1000 observations. Then, the m -th split of the data, containing the sub-matrix $\mathbf{X}_m \in \mathbb{R}^{1000 \times 500}$ and the sub-vector $\mathbf{Y}_m \in \mathbb{R}^{1000}$ is sent to the m -th GPU to compute $\mathbf{X}_m^T \mathbf{X}_m$ and $\mathbf{X}_m^T \mathbf{Y}_m$, where $m = 1, 2, \dots, 100$. Finally, these pieces are combined to get $\mathbf{X}^T \mathbf{X} = \sum_{m=1}^{100} \mathbf{X}_m^T \mathbf{X}_m$ and $\mathbf{X}^T \mathbf{Y} = \sum_{m=1}^{100} \mathbf{X}_m^T \mathbf{Y}_m$ following Section 2.5. Over 100 iterations, the average time taken for parallelly computing $\mathbf{X}_m^T \mathbf{X}_m$ and $\mathbf{X}_m^T \mathbf{Y}_m$ along with the cost of communication is only 0.17 seconds. If, on the other hand, we used the entire data in a single machine to compute $\mathbf{X}^T \mathbf{X}$ and $\mathbf{X}^T \mathbf{Y}$ directly, the average time taken over 100 replications is 18.32 seconds. Although the rest of the method, including sampling from the vanilla posterior (10000 posterior samples with a burn-in of 1000) followed by the sparsity map, is carried out on a single machine, this initial distributed computing gives quite a computational edge to our method. Moreover, the `horseshoe` package in R that implements the horseshoe method cannot allocate the huge data size and hence is rendered incapable in such scenarios. We have not tried Bayesian LASSO or SSVS in this section as we already mentioned their high computation complexity in Section 4.1. The average estimation error (MSE) for the LASSO, sparse-projection, and sparse-projection distributed are respectively 0.0017, 0.00084, and 0.00097. The average MCC in the same order is 0.923, 0.998, and 0.981.

4.3 Simulation Study 3: Polygenic Risk Score Analysis

We present a preliminary PRS study, an important real-life application of high-dimensional linear regression methods. LDpred (Vilhjálmsson et al. (2015)) that uses a spike-and-slab prior, PRS-CS (Ge et al. (2019)) that uses the Strawderman-Berger GL prior (Berger and Strawderman (1996)) and lassosum (Mak et al. (2017)) that uses a penalized regression technique are few of the commonly used methods. In addition, we implement the proposed sparse projection-posterior technique to obtain the polygenic risk scores of the phenotype of interest.

Mathematically, letting $\hat{\theta}_i$ be the effect size estimate of the i th variant obtained in the three different ways described above and G_i be the coded marker at the i th locus, we have $\text{PRS} = \sum_{i=1}^m \hat{\theta}_i G_i$. PRS analysis requires two sets of data: the target data containing individual-level genotype and phenotype data of a group of people (sample size n) and the base data comprising GWAS effect size estimates and corresponding p-values for the same phenotype and similar ancestry. The goal is to capture the phenotypic variability through SNP variability, known as SNP-heritability. The predictive power of PRS tends to increase with n . In this context, the linkage disequilibrium (LD), simply the location-based association between SNPs on the genome, should be considered for better predictions. We perform PRS-CS in `python` using the `PRScs` package (Ge et al. (2019)) and use R for both LDpred and lassosum that require packages `bigsnpr` and `bigstatsr` (Choi et al. (2020); Privé et al. (2020)). The poste-

rior mean effect size can be expressed using the LD matrix and the GWAS summary statistics within the base data in both cases. The sparse effect sizes are then used to predict the phenotype in the target data. We use quality-controlled simulated target data based on the 1000 Genomes Project European samples and a quality-controlled base GWAS data on simulated height (phenotype of interest) provided in [Choi et al. \(2020\)](#). The target data contains relevant information for 483 individuals. We divide the dataset into 21 parts, each containing 23 samples, and use 20 as training and 1 as testing. Thus, we get 21 sets of R^2 and prediction errors and plot their distributions in [Figure 5](#). The prediction accuracies of the three state-of-the-art methods seem comparable to our proposed method, with the projection method doing slightly better than the LDpred. An interesting study could check if the prediction accuracies increase when the target data sample size increases.

5 Real Data Analysis 1

First, we use the Bardet-Biedl syndrome gene expression data, an open-access dataset in the `flare` package in R. The expression data on 200 genes was collected from the eye tissue samples of 120 rats. The response is the expression data from the TRIM32 gene. The goal here is to detect the genes, if any that regulate the function of the discovered causal gene TRIM32. On applying the sparse projection-posterior method using the LASSO cross-validated penalty parameter, the MPM selects only gene 192, the only variable the LASSO selected. However, unlike the LASSO, our method is not limited to selection and estimation; instead, it quantifies the associated uncertainties. The first two plots in [Figure 6](#) show the entire induced posterior distribution of the estimated selected gene and the top-selected genes. Also, a 95% credible interval for the selected variable is obtained as (0.7553066, 0.8421185). The computation time is only ~ 13 seconds for 10000 induced posterior draws.

We consider the `riboflavin` data available in [Bühlmann et al. \(2014\)](#) for the second real data analysis. It deals with the problem of modeling the logarithm of the riboflavin production rate using the logarithm of the expression levels of $p = 4,088$ genes, observed for only $n = 71$ subjects. The only Bayesian method comparable to our proposed method is the horseshoe; the Bayesian LASSO and SSVS are too slow for high dimensions. The MPM of the horseshoe is the full model, whereas the sparse projection-posterior selects only 22 variables. Although the estimation by the horseshoe is more accurate, its model selection property lags. The LASSO selects 32 variables, and taking a queue from the simulation, we suspect the selected model could be an over-selection. To verify if the sparser model produced by the sparse projection-posterior method adequately explains the response, we studied the prediction errors in

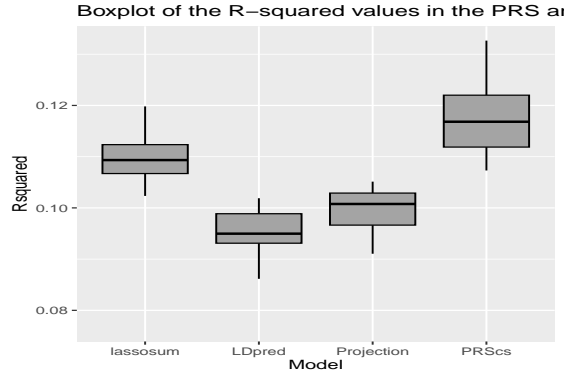


Figure 5: Boxplots of R^2 corresponding to the four competing methods.

10 random splits of the data, with 60 data points in the train set and the remaining 11 observations in the test set. The average prediction error for LASSO was 97.43, and that for the sparse projection-posterior was 90.93. The third and fourth plots in Figure 6 respectively show the full posterior distributions of the selected variables and the proportion of posterior samples containing the top 5 most selected models. We also provide the debiased-projection credible sets for the top 5 selected variables due to lack of space, noting that these can be extended to all variables. The right endpoint of these intervals is almost always 0 since their estimates are negative; hence, these intervals will likely cover the actual values.

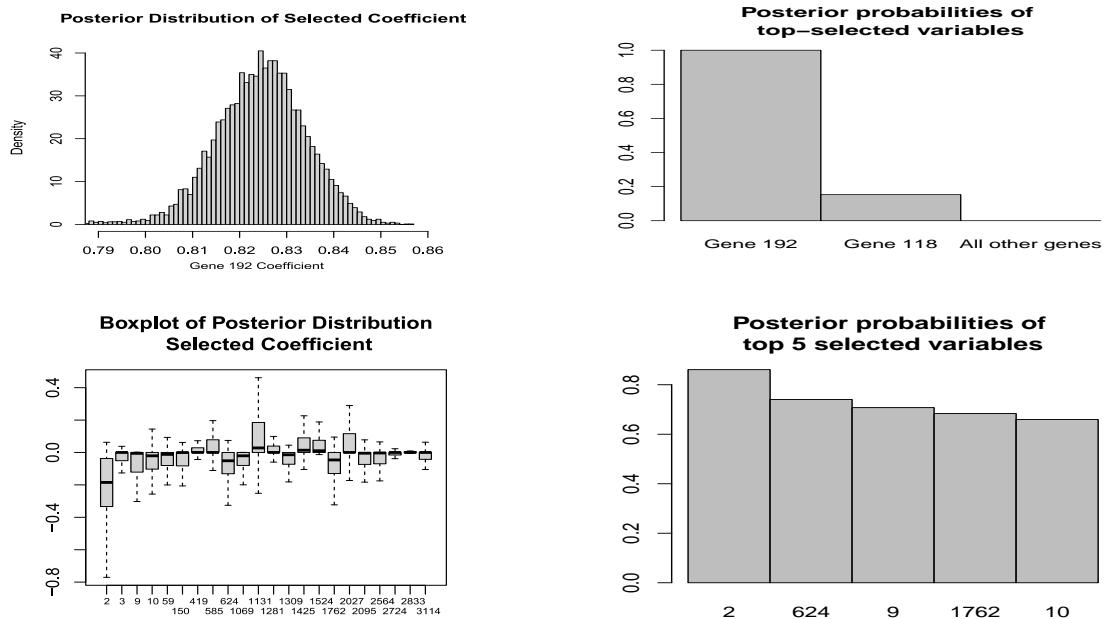


Figure 6: Posterior characteristics of the sparse projection-posterior method applied to the flare gene expression and the riboflavin data.

6 Real Data Analysis 2

We are interested to know which genes if at all any, are most significant in regulating the total Alzheimer’s Disease Assessment Scale (ADAS) cognitive scores of 729 individuals from the ADNI 2 and ADNI GO phases collected for the Alzheimer’s Disease Neuroimaging Initiative¹. The primary goal of ADNI has been to test whether serial magnetic resonance imaging (MRI), positron emission tomography (PET), other biological markers, and clinical and neuropsychological assessment can be combined to measure the progression of mild cognitive impairment (MCI) and early Alzheimer’s disease (AD). In our study, blood-based microarray expression data on 49386 genes are present. We filter the baseline ADAS data corresponding to the subjects available in the gene expression data. Previous studies have implications regarding the relation of blood-biomarker gene expression data with the stages of AD (AlMansoori et al., 2024; Lee and Lee, 2020; Li et al., 2018) using logistic LASSO or other machine learning algorithms. We identify genes based on their high association with the ADAS score. We work with the expression data using the genes retained after performing a Sure Independent Screening (SIS) pre-processing (Saldana and Feng, 2018), that removed variables having a very low correlation with the response based on some threshold. Moreover, we take this opportunity to discuss the benefit of the distributed computing property of our method. The proposed sparse projection-posterior is the only Bayesian linear regression method under sparsity to accommodate distributed computation. In real-world scenarios, data collection in different phases is quite common. We treat data from the ADNI 2 and ADNI GO phases as separate datasets. Our method only requires the summary measures of the data as explained in Section 2.5 instead of loading the entire data from all phases on a single machine. This not only reduces the burden of handling huge datasets but also respects the privacy concerns that may be associated with sharing the raw data. To see how the distributed sparse-projection method compares to existing methods and the proposed sparse-projection posterior method using the entire dataset, we report the data analysis results from the LASSO, the horseshoe, the sparse-projection, and the sparse-projection distribution.

We divide the merged ADNI GO and ADNI 2 data into test data containing 20% of the entire site and training data. The training dataset is split into two groups according to the two phases of ADNI. We capture the mean prediction errors of LASSO, the sparse-projection method, its distributed version, and the horseshoe method over 10 such random splits. The average prediction errors and their standard errors are as

¹Data used in preparation of this article were obtained from the Alzheimer’s Disease Neuroimaging Initiative (ADNI) database (<https://adni.loni.usc.edu/>). As such, the investigators within the ADNI contributed to the design and implementation of ADNI and/or provided data but did not participate in the analysis or writing of this report.

Top Selected Variables	2	624	9	1762	10
Debiased-projection credible interval	(-0.32578,0)	(-0.08465,0)	(-0.26747,0)	(-0.21748,0)	(-0.22362,0)

Table 5: Credible Intervals using the debiased-projection posterior for the top 5 most selected variables by the sparse-projection posterior method.

follows: LASSO 108.823 (28.065), sparse-projection 102.186 (26.151), sparse-projection distributed 102.309 (26.160) and finally the horseshoe 110.829 (22.123). In Figure 7, we plot the expression data corresponding to the top 30 genes with the highest average expressions across all subjects in the study in a decreasing fashion, with the left-most gene having the highest average expression. The sparse-projection and the sparse-projection distributed select the same gene as the LASSO. The selected gene is the CLIC1 gene, which is not only the highest average expressed gene across the subjects in ADNI 2 and ADNI GO as suggested by the heat plot in Figure 7, it has also been widely studied in association with Alzheimer’s disease by [Carlini et al. \(2020\)](#); [Zhang et al. \(2013\)](#); [Milton et al. \(2008\)](#); [Novarino et al. \(2004\)](#). On the other hand, the estimator of the regression coefficient obtained from the horseshoe method fails to invoke sparsity and consequently selects the full model. The 95% credible interval for the selected gene using the debiased-projection is (0.89,7.29), and the same using just the sparse-projection posterior samples is (1.30,1.34). The ADNI data analysis thus not only reiterates the relevance and effectiveness of the proposed sparse projection-posterior method and demonstrates how well it works with distributed computing.

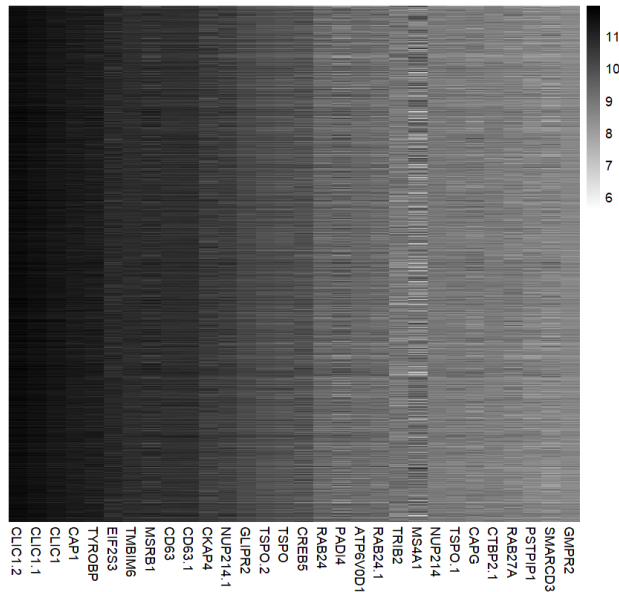


Figure 7: Heatmap of top 30 highest expressed genes.

7 Discussion

We show that the sparse projection-posterior concentrates around the true regression coefficients at an optimal rate. Our Bayesian method exhibits favorable sign-consistency, accurately selecting active predictors and determining their signs with high probability. Additionally, we establish the correct asymptotic frequentist coverage for the sparse projection-posterior credible ball through proper re-centering. The proposed method is scalable to distributed computing, efficiently handling large datasets. Simulation studies across various sample sizes and predictor dimensions support our theoretical results, revealing comparable MSE to the LASSO, correct selection of active predictors, and accurate coverage matching credibility levels in Bayesian credible sets. The extensive simulation studies show that our proposed method performs well on all these fronts. While our proposed method incurs losses in certain areas, such as a higher MSE, it compensates with strengths in others, like being comparable to LASSO and demonstrating superior MCC relative to most methods, except SSVS and SSLASSO. It excels in the coverage of credible intervals, outperforming SSVS, SSLASSO, and all other Bayesian methods, making it the best method overall. Not only in the high-dimensional penalized linear regression, this Bayesian approach shows tremendous potential in many other statistical models, where the final goal is seemingly unachievable through a traditional Bayesian method but may be easily circumvented with the help of an aptly designed projection map.

8 Acknowledgement

Data collection and sharing for the Alzheimer’s Disease Neuroimaging Initiative (ADNI) is funded by the National Institute on Aging (National Institutes of Health Grant U19 AG024904). The grantee organization is the Northern California Institute for Research and Education.

9 Funding

This research is partially supported by ARO grant number 76643MA 2020-0945.

10 Appendix

Lemma 10.1. *Under Assumption 3.4,*

$$\max_{j=1,\dots,n} \left| 1 - \frac{d_j^2}{d_j^2 + a_n} \right| = \max_{j=1,\dots,n} \left| \frac{a_n}{d_j^2 + a_n} \right| = o(n^{-1}),$$

$$\left|1 - n^{-1} \sum_{j=1}^n \frac{d_j^2}{d_j^2 + a_n}\right| = o(n^{-1}),$$

where d_1, \dots, d_n are the singular values of \mathbf{X} .

Proof. The second statement is implied by the first. By Assumption 3.4,

$$\left|1 - d_j^2/(d_j^2 + a_n)\right| \leq a_n/\min\{d_j^2 : j = 1, \dots, n\} = o(1/n),$$

uniformly for all $j = 1, \dots, n$. □

Lemma 10.2. *Under Condition 3.4, $n\hat{\sigma}_n^2 \rightarrow 0$ in probability under the true distribution, where $\hat{\sigma}_n^2$ is the usual Bayesian variance estimator $n^{-1}\mathbf{Y}^\top(\mathbf{I}_n - \mathbf{H}(a_n))\mathbf{Y}$.*

Proof. It suffices to show that the mean and the variance of the quadratic form $\mathbf{Y}^\top(\mathbf{I}_n - \mathbf{H}(a_n))\mathbf{Y}$ both tend to zero in probability. Recalling that $\mathbf{Y} = \mathbf{X}\boldsymbol{\theta}^0 + \boldsymbol{\varepsilon}$, the mean is given by $(\mathbf{X}\boldsymbol{\theta}^0)^\top(\mathbf{I}_n - \mathbf{H}(a_n))(\mathbf{X}\boldsymbol{\theta}^0)$. By Lemma 10.1, all eigenvalues of $\mathbf{I}_n - \mathbf{H}(a_n)$ are uniformly $o(n^{-1})$, while by Assumption 3.3, $\|\mathbf{X}\boldsymbol{\theta}^0\| \leq \sqrt{n}\|\mathbf{X}\boldsymbol{\theta}^0\|_\infty = o(n^{1/2})$. Thus $\mathbb{E}(\mathbf{Y}^\top(\mathbf{I}_n - \mathbf{H}(a_n))\mathbf{Y}) \rightarrow 0$. Now, $\text{var}(\mathbf{Y}^\top(\mathbf{I}_n - \mathbf{H}(a_n))\mathbf{Y})$ is

$$\begin{aligned} & \text{tr}(\mathbf{I}_n - 2\mathbf{X}(\mathbf{X}^\top\mathbf{X} + a_n\mathbf{I}_p)^{-1}\mathbf{X}^\top \\ & \quad + \mathbf{X}(\mathbf{X}^\top\mathbf{X} + a_n\mathbf{I}_p)^{-1}\mathbf{X}^\top\mathbf{X}(\mathbf{X}^\top\mathbf{X} + a_n\mathbf{I}_p)^{-1}\mathbf{X}^\top) \\ & = \sum_{j=1}^n \left(1 - 2\frac{d_j^2}{d_j^2 + a_n} + \frac{d_j^4}{(d_j^2 + a_n)^2}\right) \\ & = \sum_{j=1}^n \frac{a_n^2}{(d_j^2 + a_n)^2}, \end{aligned}$$

which is $o(n^{-1})$ by Lemma 10.1. □

Lemma 10.3. *Under Assumptions 3.1, 3.3,*

$$\Pi(\{\max_{1 \leq j \leq p} n^{-1}|\boldsymbol{\eta}^\top \mathbf{X}^{(j)}| \leq \lambda_n/2\} | \mathbf{Y}) \geq 1 - 2e^{-((C_0/4-1)\log p)/2}$$

in probability for $\lambda_n = \sigma_0\sqrt{C_0 \log p/n}$ and $C_0 > 4$.

Proof. First, we note that

$$(\boldsymbol{\eta} - \boldsymbol{\mu})^\top \mathbf{X}^{(j)} | (\mathbf{Y}, \sigma^*) \sim \mathcal{N}(0, \sigma^{*2} \mathbf{X}^{(j)\top} \mathbf{H}(a_n) \mathbf{X}^{(j)}),$$

where $\mathbf{X}^{(j)\top} \mathbf{H}(a_n) \mathbf{X}^{(j)}$ is the j th diagonal element of $\mathbf{X}^\top \mathbf{X} (\mathbf{X}^\top \mathbf{X} + a_n \mathbf{I}_p)^{-1} \mathbf{X}^\top \mathbf{X}$. Moreover, using the singular value decomposition of $\mathbf{X} = \mathbf{U} \mathbf{D} \mathbf{V}^\top$, we get

$$(\mathbf{I}_n - \mathbf{H}(a_n)) = \mathbf{U}(\mathbf{I}_p - \mathbf{D}(\mathbf{D}^2 + a_n \mathbf{I}_p)^{-1} \mathbf{D})\mathbf{U}^\top$$

and hence $(\mathbf{I}_n - \mathbf{H}(a_n))$ is non-negative definite, which in turn implies $\mathbf{X}^\top \mathbf{X} \geq \mathbf{X}^\top \mathbf{H}(a_n) \mathbf{X}$. Consequently, the magnitude of the j th diagonal element of $\mathbf{X}^\top \mathbf{X}$ will be greater than the posterior variance of $(\boldsymbol{\eta} - \boldsymbol{\mu})^\top \mathbf{X}^{(j)}$. Since \mathbf{X} is standardized to make all columns have Euclidean norm n , the diagonals of $(\mathbf{X}^\top \mathbf{X})/n$ are all 1.

Since $\Pi(\sigma^* \notin \mathcal{U}_n | \mathbf{Y}) \rightarrow 0$, it is enough to bound $\Pi(\{\max_{1 \leq j \leq p} n^{-1} |\boldsymbol{\eta}^\top \mathbf{X}^{(j)}| \leq \lambda_n/2\} | \mathbf{Y}, \sigma^*)$ by $2e^{-((C_0/4-1) \log p)/2}$ uniformly in $\sigma^* \in \mathcal{U}_n$.

Now for any $\sigma^* \in \mathcal{U}_n$,

$$\begin{aligned} & \Pi\left(\left\{\max_{1 \leq j \leq p} \frac{|(\boldsymbol{\eta} - \boldsymbol{\mu})^\top \mathbf{X}^{(j)}|}{\sigma^* \sqrt{\mathbf{X}^{(j)\top} \mathbf{H}(a_n) \mathbf{X}^{(j)}}} > \lambda_n/2\right\} | \mathbf{Y}, \sigma^*\right) \\ & \geq \Pi\left(\left\{\max_{1 \leq j \leq p} \frac{|(\boldsymbol{\eta} - \boldsymbol{\mu})^\top \mathbf{X}^{(j)}|}{\sigma^* \sqrt{n}} > \lambda_n/2\right\} | \mathbf{Y}, \sigma^*\right). \end{aligned} \quad (10.1)$$

Putting $\lambda_n = \sqrt{C_0 \log p/n}$, uniformly in $\sigma^* \in \mathcal{U}_n$, we can bound

$$\begin{aligned} & \Pi\left(\left\{\max_{1 \leq j \leq p} \frac{|(\boldsymbol{\eta} - \boldsymbol{\mu})^\top \mathbf{X}^{(j)}|}{n} \leq \sigma_0 \sqrt{\frac{C_0 \log p}{4n}}\right\} | \mathbf{Y}, \sigma^*\right) \\ & \geq 1 - \Pi\left(\left\{\max_{1 \leq j \leq p} \frac{|(\boldsymbol{\eta} - \boldsymbol{\mu})^\top \mathbf{X}^{(j)}|}{\sigma^* \sqrt{n \mathbf{X}^{(j)\top} \mathbf{H}(a_n) \mathbf{X}^{(j)}}} > \frac{\sigma_0}{\sigma^*} \sqrt{\frac{C_0 \log p}{4n}}\right\} | \mathbf{Y}, \sigma^*\right) \\ & \geq 1 - 2p \Pi\left(\frac{(\boldsymbol{\eta}^\top \mathbf{X}^{(j)} - \boldsymbol{\mu}^\top \mathbf{X}^{(j)})}{\sigma^* \sqrt{\mathbf{X}^{(j)\top} \mathbf{H}(a_n) \mathbf{X}^{(j)}}} > \frac{\sigma_0}{\sigma^* \sqrt{n}} \sqrt{\left(\frac{C_0}{4} - 1\right) \log p + \log p} \middle| \mathbf{Y}, \sigma^*\right) \\ & \geq 1 - 2 \exp\{-((C_0/4 - 1) \log p)/2\}. \end{aligned}$$

Using Assumptions 3.1 and 3.3 and the fact that the maximum of n i.i.d. Gaussian random variables grows at the $\mathcal{O}(\sqrt{\log n})$ rate, we can write

$$\begin{aligned} & \max_{1 \leq j \leq p} \frac{1}{n} |\boldsymbol{\mu}^\top \mathbf{X}^{(j)}| \\ & = \max_{1 \leq j \leq p} |\mathbf{X}^{(j)\top} \mathbf{H}(a_n) (\mathbf{X} \boldsymbol{\theta}^0 + \boldsymbol{\varepsilon}) - \mathbf{X}^{(j)\top} \mathbf{X} \boldsymbol{\theta}^0| \\ & = \max_j |\mathbf{X}^{(j)\top} \mathbf{H}(a_n) \boldsymbol{\varepsilon} - \mathbf{X}^{(j)\top} (\mathbf{I}_n - \mathbf{H}(a_n)) \mathbf{X} \boldsymbol{\theta}^0| \\ & \leq \max_j |\mathbf{X}^{(j)\top} \mathbf{H}(a_n) \boldsymbol{\varepsilon}| + \max_j |\mathbf{X}^{(j)\top} (\mathbf{I}_n - \mathbf{H}(a_n)) \mathbf{X} \boldsymbol{\theta}^0| \\ & \leq \max_j \left[\max_{1 \leq i \leq n} |\varepsilon_i| \|\mathbf{X}^{(j)\top} \mathbf{H}(a_n)\|_1 \right. \\ & \quad \left. + \max_{1 \leq i \leq n} |\mathbb{E}(Y_i)| \|\mathbf{X}^{(j)\top} (\mathbf{I}_n - \mathbf{H}(a_n))\|_1 \right], \end{aligned}$$

which is bounded above by $\mathcal{O}(\sqrt{\log n})\|\mathbf{X}^{(j)\top}\mathbf{I}_n\|_1 = \mathcal{O}(\sqrt{\log n})$. \square

Lemma 10.4. *The debiased LASSO satisfies*

$$n^{-1/2}\frac{|\mathbf{X}^{(j)\top}\mathbf{R}^{(j)}|}{\|\mathbf{R}^{(j)}\|_2}|\hat{\theta}_j^{\text{DB}} - (\theta_j^0 + m_j/\sqrt{n})| \leq A_1 + A_2,$$

where $A_1 = n^{-1/2}\|\mathbf{Y} - \mathbf{X}\hat{\boldsymbol{\theta}}^{\text{R}}\|_1$ and

$$A_2 = \sqrt{n}\lambda^{\mathbf{X}_j}\|\boldsymbol{\theta}^0 - \hat{\boldsymbol{\theta}}^L\|_1/(2\|\mathbf{R}^{(j)}\|_2).$$

Proof. We observe that

$$\begin{aligned} & n^{-1/2}\left|\frac{\mathbf{X}^{(j)\top}\mathbf{R}^{(j)}}{\|\mathbf{R}^{(j)}\|_2}[\hat{\theta}_j^{\text{DB}} - (\theta_j^0 + m_j/\sqrt{n})]\right| \\ &= n^{-1/2}\left|\frac{\mathbf{X}^{(j)\top}\mathbf{R}^{(j)}}{\|\mathbf{R}^{(j)}\|_2}\left[\frac{\mathbf{R}^{(j)\top}\mathbf{Y}}{\mathbf{R}^{(j)\top}\mathbf{X}^{(j)}} - \sum_{k \neq j} P_{jk}\hat{\theta}_k^L\right.\right. \\ &\quad \left.\left. - \theta_j^0 - \frac{\mathbf{R}^{(j)\top}\mathbf{X}\hat{\boldsymbol{\theta}}^{\text{R}}}{\mathbf{R}^{(j)\top}\mathbf{X}^{(j)}} + \sum_{k=1}^p P_{jk}\theta_k^0\right]\right| \\ &= n^{-1/2}\left|\left[\frac{\mathbf{R}^{(j)\top}(\mathbf{Y} - \mathbf{X}\hat{\boldsymbol{\theta}}^{\text{R}})}{\|\mathbf{R}^{(j)}\|_2} + \sum_{k \neq j} \frac{\mathbf{X}^{(k)\top}\mathbf{R}^{(j)}}{\|\mathbf{R}^{(j)}\|_2}(\theta_k^0 - \hat{\theta}_k^L)\right]\right| \\ &\leq n^{-1/2}\left[\max_{1 \leq i \leq n} \frac{|\mathbf{R}_i^{(j)}|/n}{\|\mathbf{R}^{(j)}\|_2/n}\|\mathbf{Y} - \mathbf{X}\hat{\boldsymbol{\theta}}^{\text{R}}\|_2\right. \\ &\quad \left.+ \max_{k \neq j} \frac{|\mathbf{R}^{(j)\top}\mathbf{X}^{(k)}|/n}{\|\mathbf{R}^{(j)}\|_2/n}\|\boldsymbol{\theta}^0 - \hat{\boldsymbol{\theta}}^L\|_1\right] \\ &\leq n^{-1/2}\left[\|\mathbf{Y} - \mathbf{X}\hat{\boldsymbol{\theta}}^{\text{R}}\|_2 + \frac{\lambda^{\mathbf{X}_j}/2}{\|\mathbf{R}^{(j)}\|_2/n}\|\boldsymbol{\theta}^0 - \hat{\boldsymbol{\theta}}^L\|_1\right], \end{aligned}$$

establishing the claim. \square

Lemma 10.5. *Under Assumption 3.4, $n^{-1/2}\|\mathbf{Y} - \mathbf{X}\hat{\boldsymbol{\theta}}^{\text{R}}\|_1 = o_P(1)$.*

Proof. Note that

$$\begin{aligned} n^{-1/2}\|\mathbf{Y} - \mathbf{X}\hat{\boldsymbol{\theta}}^{\text{R}}\|_2 &= n^{-1/2}\|(\mathbf{I}_n - \mathbf{H}(a_n))\mathbf{X}\boldsymbol{\theta}^0\|_2 \\ &\quad + n^{-1/2}\|(\mathbf{I}_n - \mathbf{H}(a_n))\boldsymbol{\varepsilon}\|_2. \end{aligned} \tag{10.2}$$

For the second summand, $E(\boldsymbol{\varepsilon}^\top(\mathbf{I}_n - \mathbf{H}(a_n))^2\boldsymbol{\varepsilon}) = \sigma^2\text{tr}((\mathbf{I}_n - \mathbf{H}(a_n))^2)$ and $\text{var}(\boldsymbol{\varepsilon}^\top(\mathbf{I}_n - \mathbf{H}(a_n))^2\boldsymbol{\varepsilon}) = \sigma^2\text{tr}((\mathbf{I}_n - \mathbf{H}(a_n))^4)$. Since $(\mathbf{I}_n - \mathbf{H}(a_n))$ is non-negative definite, by Lemma 10.1, $\text{tr}((\mathbf{I}_n - \mathbf{H}(a_n))^2) \leq \text{tr}(\mathbf{I}_n - \mathbf{H}(a_n)) = o(1)$, and similarly, $\text{tr}((\mathbf{I}_n - \mathbf{H}(a_n))^4) = o(1)$. Consequently, $n^{-1/2}\|(\mathbf{I}_n - \mathbf{H}(a_n))\boldsymbol{\varepsilon}\|_2 = o(n^{-1/2})$.

Referring to $(\mathbf{A})_{i,j}$ as the element in the i th row and j th column of a matrix $\mathbf{A} \in \mathbb{R}^{n \times n}$, we can bound the first term $n^{-1/2} \|(\mathbf{I}_n - \mathbf{H}(a_n)) \mathbf{X} \boldsymbol{\theta}^0\|_2$ in (10.2) by

$$n^{-1/2} \|\mathbf{X} \boldsymbol{\theta}^0\|_2 \left(\sum_{i=1}^n \sum_{j=1}^n (\mathbf{I}_n - \mathbf{H}(a_n))_{i,j}^2 \right)^{1/2}$$

using the Cauchy-Schwartz inequality. Finally, this upper bound is $\left\{ \text{tr}(\mathbf{I}_n - \mathbf{H}(a_n))^2 \right\}^{1/2} = o(1)$. \square

Let $\hat{\boldsymbol{\theta}}_{S_0}^{\text{R,PS}} = (\mathbf{X}_{(1)}^T \mathbf{X}_{(1)} + a_n \mathbf{I}_{s_0})^{-1} \mathbf{X}_{(1)}^T \mathbf{Y}$ stand for the ridge regression estimator with predictors restricted to S_0 post selection of model S_0 .

Lemma 10.6. *If the S_0 is fixed and $\mathbf{C}_{n(11)} \rightarrow \mathbf{C}_{(11)}$ as $n \rightarrow \infty$, then under Assumptions 3.1, $\sqrt{n}(\hat{\boldsymbol{\theta}}_{S_0}^{\text{R,PS}} - \boldsymbol{\theta}_{S_0}^0) \rightsquigarrow \mathcal{N}_{s_0}(\mathbf{0}_{s_0}, \sigma_0^2 \mathbf{C}_{(11)}^{-1})$.*

Proof. Without loss of generality, let the first s_0 components correspond to signal variables. Since $n^{-1}(\mathbf{X}_{(1)}^T \mathbf{X}_{(1)} + a_n \mathbf{I}_{s_0}) \rightarrow \mathbf{C}_{(11)}$, it suffices to prove that $n^{-1/2} \mathbf{X}_{(1)}^T \boldsymbol{\varepsilon} \rightsquigarrow \mathcal{N}_{s_0}(0, \sigma_0^2 \mathbf{C}_{(11)})$.

Let $\mathbf{0} \neq \mathbf{b} \in \mathbb{R}^{s_0}$ be fixed. Because of the Cramér-Wold device, it is enough to note that the variance term

$$\begin{aligned} & \text{cov}\left(n^{-1/2} \sum_{j=1}^{s_0} \sum_{i=1}^n b_j x_{ij} \varepsilon_i, n^{-1/2} \sum_{j=1}^{s_0} \sum_{i=1}^n x_{ik} \varepsilon_i\right) \\ &= \sigma_0^2 n^{-1} \sum_{j=1}^{s_0} \sum_{k=1}^{s_0} \sum_{i=1}^n x_{ij} x_{ik} b_j b_k \rightarrow \sigma_0^2 \mathbf{b}^T \mathbf{C} \mathbf{b}, \end{aligned}$$

and verify the conditions of Lindeberg's central limit theorem (CLT) for $n^{-1/2} \mathbf{b}^T \mathbf{X}_{(1)}^T \boldsymbol{\varepsilon}$. Since $\boldsymbol{\varepsilon}$ has i.i.d. components, Lindeberg's condition reduces to

$$\frac{n^{-1} \max_i (\sum_{j=1}^{s_0} b_j x_{ij})^2}{n^{-1} \sum_{i=1}^n (\sum_{j=1}^{s_0} b_j x_{ij})^2} \rightarrow 0.$$

This holds since

$$\begin{aligned} \frac{n^{-1} \max_i (\sum_{j=1}^{s_0} b_j x_{ij})^2}{n^{-1} \sum_{i=1}^n (\sum_{j=1}^{s_0} b_j x_{ij})^2} &\leq \frac{\|\mathbf{b}\|^2 n^{-1} \max_i \sum_{j=1}^{s_0} x_{ij}^2}{n^{-1} \|\mathbf{b}^T \mathbf{X}_{(1)}\|^2} \\ &\leq \frac{\|\mathbf{b}\|^2 n^{-1} s_0 M_1^2}{\mathbf{b}^T \mathbf{C}_{n(11)} \mathbf{b}} \rightarrow 0, \end{aligned}$$

as $\mathbf{b}^T \mathbf{C}_{n(11)} \mathbf{b} \rightarrow \mathbf{b}^T \mathbf{C}_{(11)} \mathbf{b} > 0$ for any $\mathbf{b} \neq \mathbf{0}$ by the positive definiteness of $\mathbf{C}_{(11)}$. \square

Proof of Theorem 3.1. From (2.4), since $\boldsymbol{\theta}^*$ is the minimizer, we can write

$$\frac{1}{2n} \|\mathbf{X} \boldsymbol{\theta} - \mathbf{X} \boldsymbol{\theta}^0\|_2^2 + \lambda_n \|\boldsymbol{\theta}^0\|_1$$

$$\begin{aligned}
&\geq \frac{1}{2n} \|\mathbf{X}\boldsymbol{\theta} - \mathbf{X}\boldsymbol{\theta}^*\|_2^2 + \lambda_n \|\boldsymbol{\theta}^*\|_1 \\
&= \frac{1}{2n} \|\mathbf{X}\boldsymbol{\theta}^0 + \boldsymbol{\eta} - \mathbf{X}\boldsymbol{\theta}^*\|_2^2 + \lambda_n \|\boldsymbol{\theta}^*\|_1 \\
&= \frac{1}{2n} \|\mathbf{X}\boldsymbol{\theta}^0 - \mathbf{X}\boldsymbol{\theta}^*\|_2^2 + \frac{1}{2n} \|\boldsymbol{\eta}\|_2^2 \\
&\quad - \frac{1}{n} \boldsymbol{\eta}^\top \mathbf{X}(\boldsymbol{\theta}^0 - \boldsymbol{\theta}^*) + \lambda_n \|\boldsymbol{\theta}^*\|_1. \tag{10.3}
\end{aligned}$$

Given the j th column of \mathbf{X} , define a set $E_n = \{\max_{1 \leq j \leq p} n^{-1} |\boldsymbol{\eta}^\top \mathbf{X}^{(j)}| \leq \lambda_0\}$ for some constant λ_0 . Then, following Lemma 10.3 on this set, (10.3) implies

$$\begin{aligned}
&\frac{1}{2n} \|\mathbf{X}\boldsymbol{\theta}^0 - \mathbf{X}\boldsymbol{\theta}^*\|_2^2 + \lambda_n \|\boldsymbol{\theta}^*\|_1 \\
&\leq n^{-1} \boldsymbol{\eta}^\top \mathbf{X}(\boldsymbol{\theta}^0 - \boldsymbol{\theta}^*) + \lambda_n \|\boldsymbol{\theta}^0\|_1 \\
&\leq \max_{1 \leq j \leq p} \frac{|\boldsymbol{\eta}^\top \mathbf{X}^{(j)}|}{n} \|\boldsymbol{\theta}^0 - \boldsymbol{\theta}^*\|_1 + \lambda_n \|\boldsymbol{\theta}^0\|_1.
\end{aligned}$$

which is bounded by $\lambda_0 \|\boldsymbol{\theta}^0 - \boldsymbol{\theta}^*\|_1 + \lambda_n \|\boldsymbol{\theta}^0\|_1$. After decomposing the vectors into components $\boldsymbol{\theta}_{S_0}$ and $\boldsymbol{\theta}_{S_0^c}$ corresponding to the oracle set S_0 and its complement, we have by the triangle inequality that $\|\boldsymbol{\theta}_{S_0}^* - \boldsymbol{\theta}_{S_0}^0\|_1 \geq \|\boldsymbol{\theta}_{S_0}^0\|_1 - \|\boldsymbol{\theta}_{S_0}^*\|_1$. Since $\boldsymbol{\theta}_{S_0^c}^0 = \mathbf{0}_{p-s_0}$, by choosing $\lambda_0 \leq \lambda_n/2$, we can rewrite the above inequality as

$$\begin{aligned}
\frac{1}{2n} \|\mathbf{X}\boldsymbol{\theta}^0 - \mathbf{X}\boldsymbol{\theta}^*\|_2^2 &\leq \frac{\lambda_n}{2} (\|\boldsymbol{\theta}_{S_0}^0 - \boldsymbol{\theta}_{S_0}^*\|_1 + \|\boldsymbol{\theta}_{S_0^c}^0\|_1) \\
&\quad + \lambda_n (\|\boldsymbol{\theta}_{S_0}^0\|_1 - \|\boldsymbol{\theta}_{S_0}^*\|_1 - \|\boldsymbol{\theta}_{S_0^c}^*\|_1),
\end{aligned}$$

which implies that

$$\frac{1}{2n} \|\mathbf{X}\boldsymbol{\theta}^0 - \mathbf{X}\boldsymbol{\theta}^*\|_2^2 + \frac{\lambda_n}{2} \|(\boldsymbol{\theta}^* - \boldsymbol{\theta}^0)_{S_0^c}\|_1 \leq \frac{3\lambda_n}{2} \|(\boldsymbol{\theta}^* - \boldsymbol{\theta}^0)_{S_0}\|_1.$$

Then, making use of the compatibility condition, we arrive at the relation

$$\begin{aligned}
\frac{1}{2n} \|\mathbf{X}\boldsymbol{\theta}^0 - \mathbf{X}\boldsymbol{\theta}^*\|_2^2 + \frac{\lambda_n}{2} \|\boldsymbol{\theta}^* - \boldsymbol{\theta}^0\|_1 &\leq 2\lambda_n \|(\boldsymbol{\theta}^* - \boldsymbol{\theta}^0)_{S_0}\|_1 \\
&\leq \frac{2\lambda_n \sqrt{s_0}}{\sqrt{n}\phi_0} \|\mathbf{X}\boldsymbol{\theta}^0 - \mathbf{X}\boldsymbol{\theta}^*\|_2.
\end{aligned}$$

Finally, using $2ab \leq a^2 + b^2$ with $a = 1/(2\sqrt{n}) \|\mathbf{X}\boldsymbol{\theta}^0 - \mathbf{X}\boldsymbol{\theta}^*\|_2$ and $b = \lambda_n \sqrt{s_0}/\phi_0$, we can bound the above as

$$\frac{1}{4n} \|\mathbf{X}\boldsymbol{\theta}^0 - \mathbf{X}\boldsymbol{\theta}^*\|_2^2 + \frac{\lambda_n}{2} \|\boldsymbol{\theta}^* - \boldsymbol{\theta}^0\|_1 \leq \frac{4\lambda_n^2 s_0}{\phi_0^2},$$

which implies that $\|\boldsymbol{\theta}^* - \boldsymbol{\theta}^0\|_1 = \mathcal{O}_P(s_0 \lambda_n)$. \square

Proof of Theorem 3.2. We can write $\boldsymbol{\theta}^*$ as,

$$\begin{aligned} & \arg \min_{\mathbf{u}} \{ \|\mathbf{X}\boldsymbol{\theta} - \mathbf{X}\mathbf{u}\|_2^2 + n\lambda_n \|\mathbf{u}\|_1 \} \\ & = \arg \min_{\mathbf{u}} \{ \|\mathbf{X}\boldsymbol{\theta} - \mathbf{X}\boldsymbol{\theta}^0 - \mathbf{X}(\mathbf{u} - \boldsymbol{\theta}^0)\|_2^2 + n\lambda_n \|\mathbf{u} - \boldsymbol{\theta}^0 + \boldsymbol{\theta}^0\|_1 \}. \end{aligned}$$

Hence $\mathbf{u}_1^* = \boldsymbol{\theta}^* - \boldsymbol{\theta}^0$ is given by

$$\begin{aligned} & \arg \min_{\mathbf{u}_1} \{ \|\boldsymbol{\eta} - \mathbf{X}\mathbf{u}_1\|_2^2 + n\lambda_n \|\mathbf{u}_1 + \boldsymbol{\theta}^0\|_1 \} \\ & = \arg \min_{\mathbf{u}_1} \{ \mathbf{u}_1^\top \mathbf{X}^\top \mathbf{X} \mathbf{u}_1 - 2\mathbf{u}_1^\top \mathbf{X}^\top \boldsymbol{\eta} + n\lambda_n \sum_{j=1}^p |\theta_j^0 + u_{1j}| \}. \end{aligned} \quad (10.4)$$

Differentiating $\mathbf{u}_1^\top \mathbf{X}^\top \mathbf{X} \mathbf{u}_1 - \mathbf{u}_1^\top \mathbf{X}^\top \boldsymbol{\eta}$ with respect to \mathbf{u}_1 , we get,

$$[2\mathbf{X}^\top \mathbf{X} \mathbf{u}_1 - 2\mathbf{X}^\top \boldsymbol{\eta}] = 2\sqrt{n} \{ \mathbf{C}_n(\sqrt{n}\mathbf{u}_1) - \mathbf{Z}_n \}, \quad (10.5)$$

where

$$\mathbf{Z}_n := n^{-1/2} \mathbf{X}^\top \boldsymbol{\eta} = n^{-1/2} \begin{bmatrix} \mathbf{X}_{n(1)}^\top \boldsymbol{\eta} \\ \mathbf{X}_{n(2)}^\top \boldsymbol{\eta} \end{bmatrix} = \begin{bmatrix} \mathbf{Z}_{n(1)} \\ \mathbf{Z}_{n(2)} \end{bmatrix}.$$

To find a solution to (10.4), the Karush-Kuhn-Tucker (KKT) conditions are employed. These represent a set of initial derivative tests, often referred to as first-order necessary conditions, to determine the optimality of a solution in a constrained optimization problem, assuming that specific regularity conditions are met. The stationarity condition that the gradient of the generalized Lagrangian given in (10.5) is zero at the minimizer \mathbf{u}_1^* is characterized by

$$2\sqrt{n} \{ \mathbf{C}_n(\sqrt{n}\mathbf{u}_1) - \mathbf{Z}_n \} = -n\lambda_n \boldsymbol{\gamma},$$

where $\boldsymbol{\gamma} = (\gamma_1, \dots, \gamma_p)^\top$ is the subdifferential given by

$$\gamma_j \in \begin{cases} \text{sign}(\theta_j^*), & \text{if } \theta_j^* \neq 0 \text{ for } j \leq s_0, \\ [-1, 1], & \text{if } \theta_j^* = 0 \text{ for } j > s_0. \end{cases}$$

Let $\boldsymbol{\theta}^* = \begin{bmatrix} \boldsymbol{\theta}_{(1^*)}^* \\ \boldsymbol{\theta}_{(2^*)}^* \end{bmatrix}$ be the partition of the sparse projection where $\boldsymbol{\theta}_{(1^*)}^*$ consists of all non-zero elements of $\boldsymbol{\theta}^*$ and $\boldsymbol{\theta}_{(2^*)}^*$ is the collection of the zero components. This partition is different from the original partition of the data-generating truth $\boldsymbol{\theta}^0 =$

$\begin{bmatrix} \boldsymbol{\theta}_{(1)}^0 \\ \boldsymbol{\theta}_{(2)}^0 \end{bmatrix}$. Then, we can partition the associated matrices and vectors of (10.5) as

$$2\sqrt{n} \left\{ \begin{bmatrix} \mathbf{C}_{n(11^*)} & \mathbf{C}_{n(12^*)} \\ \mathbf{C}_{n(21^*)} & \mathbf{C}_{n(22^*)} \end{bmatrix} \sqrt{n} \begin{bmatrix} \mathbf{u}_{1(1^*)}^* \\ \mathbf{u}_{1(2^*)}^* \end{bmatrix} - \begin{bmatrix} \mathbf{Z}_{n(1^*)} \\ \mathbf{Z}_{n(2^*)} \end{bmatrix} \right\}.$$

Following the KKT conditions, we have

- (a) $\sum_{k=1}^2 \mathbf{C}_{n(1k^*)} [\sqrt{n} \mathbf{u}_{1(k^*)}^*] - \mathbf{Z}_{n(1^*)} = -\frac{\sqrt{n}\lambda_n}{2} \text{sign}(\boldsymbol{\theta}_{(1)}^*)$,
- (b) $|\mathbf{C}_{n(21^*)} [\sqrt{n} \mathbf{u}_{1(1^*)}^*] + \mathbf{C}_{n(22^*)} [\sqrt{n} \mathbf{u}_{1(2^*)}^*] - \mathbf{Z}_{n(2^*)}| \leq \frac{\sqrt{n}\lambda_n}{2} \mathbf{1}$.

For the event $\{\text{sign}(\boldsymbol{\theta}^*) = \text{sign}(\boldsymbol{\theta}^0)\}$ to happen, the partition of $\boldsymbol{\theta}^*$ and $\boldsymbol{\theta}^0$ should match. That is, if the sparse projection selects the variables correctly, then $\mathbf{u}_{1(2^*)}^* = \boldsymbol{\theta}_{(2^*)}^* - \boldsymbol{\theta}_{(2)}^0 = \boldsymbol{\theta}_{(2)}^* - \boldsymbol{\theta}_{(2)}^0 = \mathbf{0}$ and $\text{sign}(\boldsymbol{\theta}_{(1)}^0) = \text{sign}(\boldsymbol{\theta}_{(1)}^*)$. Then, the revised KKT conditions, along with an added condition listed below, imply sign consistency of the sparse projection. That is, if

- (i) $\mathbf{C}_{n(11)} [\sqrt{n} \mathbf{u}_{1(1)}^*] - \mathbf{Z}_{n(1)} = -\frac{\sqrt{n}\lambda_n}{2} \text{sign}(\boldsymbol{\theta}_{(1)}^0)$,
 - (ii) $|\mathbf{C}_{n(21)} [\sqrt{n} \mathbf{u}_{1(1)}^*] - \mathbf{Z}_{n(2)}| \leq \frac{\sqrt{n}\lambda_n}{2} \mathbf{1}$,
 - (iii) $\{|\mathbf{u}_{1(1)}^*| < |\boldsymbol{\theta}_{(1)}^0|\} \subseteq \{\text{sign}(\boldsymbol{\theta}_{(1)}^*) = \text{sign}(\boldsymbol{\theta}_{(1)}^0)\}$,
- then, the events in (i), (ii), (iii) together imply $\{\text{sign}(\boldsymbol{\theta}_{(1)}^*) = \text{sign}(\boldsymbol{\theta}_{(1)}^0)\} = \{\text{sign}(\boldsymbol{\theta}^*) = \text{sign}(\boldsymbol{\theta}^0)\}$ and

$$\begin{aligned} & \Pi(\{\text{sign}(\boldsymbol{\theta}^*) = \text{sign}(\boldsymbol{\theta}^0)\} | \mathbf{Y}) \\ & \geq \Pi(\{\mathbf{C}_{n(11)} [\sqrt{n} \mathbf{u}_{1(1)}^*] - \mathbf{Z}_{n(1)} = -\frac{\sqrt{n}\lambda_n}{2} \text{sign}(\boldsymbol{\theta}_{(1)}^0)\}) \\ & \quad \cap \{|\mathbf{u}_{1(1^*)}^*| < |\boldsymbol{\theta}_{(1)}^0|\} \\ & \quad \cap \{|\mathbf{C}_{n(21)} [\sqrt{n} \mathbf{u}_{1(1)}^*] - \mathbf{Z}_{n(2)}| \leq \frac{\sqrt{n}\lambda_n}{2} \mathbf{1}\} | \mathbf{Y}) \\ & = \Pi(\{|\mathbf{C}_{n(11)}^{-1} (\mathbf{Z}_{n(1)} - \frac{\sqrt{n}\lambda_n}{2} \text{sign}(\boldsymbol{\theta}_{(1)}^0))| \leq \sqrt{n} |\boldsymbol{\theta}_{(1)}^0|\}) \\ & \quad \cap \{|\mathbf{C}_{n(21)} \mathbf{C}_{n(11)}^{-1} \mathbf{Z}_{n(1)} - \mathbf{Z}_{n(2)}| \\ & \quad \leq \frac{\sqrt{n}\lambda_n}{2} (\mathbf{1} - |\mathbf{C}_{n(21)} \mathbf{C}_{n(11)}^{-1} \text{sign}(\boldsymbol{\theta}_{(1)}^0)|)\} | \mathbf{Y}) \\ & = \Pi(A_n \cap \tilde{B}_n | \mathbf{Y}), \end{aligned}$$

where, by the irrerepresentable condition in Assumption 3.7,

$$\begin{aligned} \tilde{B}_n & := \{|\mathbf{C}_{n(21)} \mathbf{C}_{n(11)}^{-1} \mathbf{Z}_{n(1)} - \mathbf{Z}_{n(2)}| \\ & \leq \frac{\sqrt{n}\lambda_n}{2} (\mathbf{1} - |\mathbf{C}_{n(21)} \mathbf{C}_{n(11)}^{-1} \text{sign}(\boldsymbol{\theta}_{(1)}^0)|)\} \supseteq B_n. \end{aligned}$$

On the event B_n , every component of the vector on the left-hand side of the inequality

is less than the respective component of the vector on the right-hand side. Then, we conclude that

$$\begin{aligned}\Pi(\{\text{sign}(\boldsymbol{\theta}^*) = \text{sign}(\boldsymbol{\theta}^0)\}|\mathbf{Y}) &\geq \Pi(A_n \cap B_n|\mathbf{Y}) \\ &= 1 - [\Pi(A_n^c|\mathbf{Y}) + \Pi(B_n^c|\mathbf{Y})].\end{aligned}$$

Define the following quantities

$$\begin{aligned}\mathbf{W}_{1n} &= n^{-1/2}\mathbf{C}_{n(11)}^{-1}\mathbf{X}_{n(1)}^\top, \\ \mathbf{V}_1 &= n^{-1}\sigma^2\mathbf{C}_{n(11)}^{-1}\mathbf{X}_{n(1)}^\top\mathbf{H}(a_n)\mathbf{X}_{n(1)}\mathbf{C}_{n(11)}^{-1}, \\ \mathbf{W}_{2n} &= n^{-1/2}(\mathbf{C}_{n(21)}\mathbf{C}_{n(11)}^{-1}\mathbf{X}_{n(1)}^\top - \mathbf{X}_{n(2)}^\top), \\ \mathbf{V}_2 &= \mathbf{C}_{n(21)}\mathbf{V}_1\mathbf{C}_{n(21)} - n^{-1}\sigma^2\mathbf{X}_{n(2)}^\top\mathbf{H}(a_n)\mathbf{X}_{n(2)},\end{aligned}$$

where $\mathbf{W}_{2n} \in \mathbb{R}^{(p-s_0) \times n}$. Given the data, we have

$$\begin{aligned}\mathbf{C}_{n(11)}^{-1}\mathbf{Z}_{n(1)}|\mathbf{Y} &\sim \mathcal{N}_{s_0}(\mathbf{W}_{1n}\boldsymbol{\mu}, \mathbf{V}_1), \\ \mathbf{C}_{n(21)}\mathbf{C}_{n(11)}^{-1}\mathbf{Z}_{n(1)} - \mathbf{Z}_{n(2)}|\mathbf{Y} &\sim \mathcal{N}_{p-s_0}(\mathbf{W}_{2n}\boldsymbol{\mu}, \mathbf{V}_2).\end{aligned}$$

Let $\mathbf{W}_{2n} = (\mathbf{w}_{2n}^{(1)}, \dots, \mathbf{w}_{2n}^{(p-s_0)})^\top$ such that $\mathbf{w}_{2n}^{(j)} \in \mathbb{R}^n$ for all $j = 1, \dots, p - s_0$. Thus, the individual components of both vectors defined above have finite variances. Then, defining a_{nj} as the j th component of the s_0 -dimensional vector $\mathbf{C}_{n(11)}^{-1}\mathbf{Z}_{n(1)} - \mathbf{W}_{1n}\boldsymbol{\mu}$ and b_{nj} as the j th component of $\mathbf{C}_{n(21)}\mathbf{C}_{n(11)}^{-1}\mathbf{Z}_{n(1)} - \mathbf{Z}_{n(2)} - \mathbf{W}_{2n}\boldsymbol{\mu}$, we have, $\sup_{\sigma^* \in \mathcal{U}_n} \mathbb{E}(a_{nj}|\mathbf{Y}, \sigma^*)^2 < h^2$, and $\sup_{\sigma^* \in \mathcal{U}_n} \mathbb{E}(b_{nj}|\sigma^*, \mathbf{Y})^2 < h^2$ for some constant $h > 0$. Then with P_1 and P_2 defined by

$$P_1 = \left\| \frac{\sqrt{n}\lambda_n}{2}\mathbf{C}_{n(11)}^{-1}\text{sign}(\boldsymbol{\theta}_{(1)}^0) \right\|_2, \quad P_2 = \|\mathbf{W}_{1n}\boldsymbol{\mu}\|_\infty,$$

we have,

$$\begin{aligned}&\sup_{\sigma^* \in \mathcal{U}_n} \Pi(A_n^c|\mathbf{Y}, \sigma^*) \\ &= \sup_{\sigma^* \in \mathcal{U}_n} \Pi(\{\|\mathbf{C}_{n(11)}^{-1}\mathbf{Z}_{n(1)} - \frac{\sqrt{n}\lambda_n}{2}\mathbf{C}_{n(11)}^{-1}\text{sign}(\boldsymbol{\theta}_{(1)}^0)\|_\infty \\ &\quad > \sqrt{n}(\|\boldsymbol{\theta}_{(1)}^0\|_{\min})\}|\mathbf{Y}, \sigma^*) \\ &\leq \sup_{\sigma^* \in \mathcal{U}_n} \Pi(\{\|\mathbf{C}_{n(11)}^{-1}\mathbf{Z}_{n(1)} - \mathbf{W}_{1n}\boldsymbol{\mu}\|_\infty \\ &\quad + \|\frac{\sqrt{n}\lambda_n}{2}\mathbf{C}_{n(11)}^{-1}\text{sign}(\boldsymbol{\theta}_{(1)}^0)\|_\infty \\ &\quad + \|\mathbf{W}_{1n}\boldsymbol{\mu}\|_\infty > \sqrt{n}(\|\boldsymbol{\theta}_{(1)}^0\|_{\min})\}|\mathbf{Y}, \sigma^*) \\ &\leq \Pi(P_1 + P_2 > \frac{\sqrt{n}}{2}\|\boldsymbol{\theta}_{(1)}^0\|_{\min}|\mathbf{Y})\end{aligned}$$

$$\begin{aligned}
& + \sup_{\sigma^* \in \mathcal{U}_n} \Pi\left(\bigcup_{j=1}^{s_0} \{|a_{nj}| > \frac{\sqrt{n}}{2} \|\boldsymbol{\theta}_j^0\|_{\min}\} \mid \mathbf{Y}, \sigma^*\right) \\
& \leq \Pi\left(\frac{\sqrt{n}\lambda_n\sqrt{s_0}}{M_2} + \|\mathbf{W}_{1n}\boldsymbol{\mu}\|_{\infty} > \frac{\sqrt{n}}{2} \|\boldsymbol{\theta}_{(1)}^0\|_{\min} \mid \mathbf{Y}\right) \\
& \quad + \sum_{j=1}^{s_0} \sup_{\sigma^* \in \mathcal{U}_n} \Pi(|a_{nj}| > \frac{M_3}{2} n^{b_2/2} \mid \mathbf{Y}, \sigma^*) \tag{10.6}
\end{aligned}$$

by the beta-min condition. Now,

$$\begin{aligned}
& \Pi\left(\frac{\sqrt{n}\lambda_n\sqrt{s_0}}{M_2} + \|\mathbf{W}_{1n}\boldsymbol{\mu}\|_{\infty} > \frac{\sqrt{n}}{2} \|\boldsymbol{\theta}_{(1)}^0\|_{\min}\right) \\
& \leq \Pi\left(\|\mathbf{W}_{1n}\|_F \|\mathbf{X}(\hat{\boldsymbol{\theta}}^R - \boldsymbol{\theta}_0)\|_2 > \frac{\sqrt{n}}{2} \|\boldsymbol{\theta}_{0(1)}\|_{\min} + b_0 n^{\frac{b_4+b_1}{2}}\right) \\
& \leq \frac{\|\mathbf{C}_{n(11)}^{-1} \mathbf{X}_{n(1)}^T\|_F^2 \mathbb{E}(n^{-1} \|\mathbf{X}\hat{\boldsymbol{\theta}}^R - \mathbf{X}\boldsymbol{\theta}_0\|_2^2)}{(\sqrt{n}\|\boldsymbol{\theta}_{0(1)}\|_{\min}/2 + b_0 n^{(b_4+b_1)/2})^2}
\end{aligned}$$

for some constant $b_0 > 0$. Clearly, first term in (10.6) is free of σ^* and goes to zero since $\sqrt{n}2\|\boldsymbol{\theta}_{0(1)}\|_{\min}/2$ grows to infinity faster than $n^{b_2/2}$ and by the theory of ridge regression estimation in [Shao and Deng \(2012\)](#), we have $\mathbb{E}(\|\mathbf{X}\hat{\boldsymbol{\theta}}^R - \mathbf{X}\boldsymbol{\theta}_0\|_2^2) = \mathcal{O}(n)$. The second term of (10.6) reduces to $s_0 \mathcal{O}(1 - \Phi((2h)^{-1}M_3 n^{b_2/2})) = o(e^{-n^{b_3}})$ using the Gaussian tail bound $1 - \Phi(t) \leq t^{-1}e^{-t^2/2}$. Next, writing $\nu_* = \min\{\nu_j : 1 \leq j \leq p - s_0\}$, we have,

$$\begin{aligned}
& \sup_{\sigma^* \in \mathcal{U}_n} \Pi(B_n^c \mid \mathbf{Y}, \sigma^*) \\
& = \Pi\left(\left\{|\mathbf{C}_{n(21)}\mathbf{C}_{n(11)}^{-1}\mathbf{Z}_{n(1)} - \mathbf{Z}_{n(2)}| > \frac{\sqrt{n}\lambda_n}{2}\boldsymbol{\nu}\right\} \mid \mathbf{Y}, \sigma^*\right) \\
& \leq \sup_{\sigma^* \in \mathcal{U}_n} \Pi\left(\left\{|\mathbf{C}_{n(21)}\mathbf{C}_{n(11)}^{-1}\mathbf{Z}_{n(1)} - \mathbf{Z}_{n(2)} - \mathbf{W}_{2n}\boldsymbol{\mu}| \right. \right. \\
& \quad \left. \left. + |\mathbf{W}_{2n}\boldsymbol{\mu}| > \frac{\sqrt{n}\lambda_n}{2}\boldsymbol{\nu}\right\} \mid \mathbf{Y}, \sigma^*\right) \\
& \leq \sup_{\sigma^* \in \mathcal{U}_n} \Pi\left(\bigcup_{j=1}^{p-s_0} \{|b_{nj}| > \frac{\sqrt{n}\lambda_n}{2}\nu_j\} \mid \mathbf{Y}, \sigma^*\right) \\
& \quad + \Pi(|\mathbf{W}_{2n}\boldsymbol{\mu}| > \frac{\sqrt{n}\lambda_n}{2}\boldsymbol{\nu} \mid \mathbf{Y}) \\
& \leq \sup_{\sigma^* \in \mathcal{U}_n} \Pi\left(\bigcup_{j=1}^{p-s_0} \{|b_{nj}| > \frac{\sqrt{n}\lambda_n}{2}\nu_*\} \mid \mathbf{Y}, \sigma^*\right) \\
& \quad + \Pi(\|\mathbf{W}_{2n}\|_F \|\mathbf{X}(\hat{\boldsymbol{\theta}}_R - \boldsymbol{\theta}_0)\|_2 > \frac{\sqrt{n}\lambda_n}{2}\boldsymbol{\nu} \mid \mathbf{Y}) \\
& \leq \sum_{j=1}^{p-s_0} \sup_{\sigma^* \in \mathcal{U}_n} \Pi\left(\{|b_{nj}| > \frac{\sqrt{n}\lambda_n}{2}\nu_*\} \mid \mathbf{Y}, \sigma^*\right)
\end{aligned}$$

$$\begin{aligned}
& + \frac{\|\mathbf{W}_{2n}\|_F^2 \|\mathbf{X}(\hat{\boldsymbol{\theta}}_R - \boldsymbol{\theta}_0)\|_2^2}{\left(\frac{\lambda_n}{2\sqrt{n}}\boldsymbol{\nu}\right)^2} \\
& = (p - s_0)\mathcal{O}\left(1 - \Phi\left(\frac{\sqrt{n}\lambda_n\nu_*}{2h}\right)\right) \\
& + \frac{\|\mathbf{C}_{n(21)}\mathbf{C}_{n(11)}^{-1}\mathbf{X}_{n(1)}^\top - \mathbf{X}_{n(2)}^\top\|_F^2 \mathbb{E}\left(\frac{1}{n}\|\mathbf{X}(\hat{\boldsymbol{\theta}}_R - \boldsymbol{\theta}_0)\|_2^2\right)}{\left(\frac{\sqrt{n}\lambda_n}{2}\boldsymbol{\nu}\right)^2}.
\end{aligned}$$

Again, the second term goes to zero as the denominator grows like n^{b_4} , whereas the numerator is $\mathcal{O}(1)$, and the first term is $\mathcal{O}(pe^{-n\lambda_n^2\nu_*^2/(2h)}) = o(e^{n^{b_3}})$ by the Gaussian tail bound because $n\lambda_n^2 \asymp n^{b_4} \gg n^{b_3}$. Consequently, we have $\Pi(B_n^\epsilon|\mathbf{Y}) \leq o(e^{-n^{b_3}})$. \square

Proof of Theorem 3.3. Using (3.4), decompose $\sqrt{n}(\theta_j^{**} - \theta_j^0) = T_j + \Lambda_j$, where where

$$T_j = \sqrt{n}\left(\frac{\mathbf{R}^{(j)\top}\mathbf{X}\boldsymbol{\theta}}{\mathbf{R}^{(j)\top}\mathbf{X}^{(j)}} - \sum_{k=1}^p P_{jk}\theta_k^0\right)$$

is the fluctuation term, and

$$\Lambda_j = \sqrt{n}\sum_{k \neq j} P_{jk}(\theta_k^0 - \theta_k^*)$$

is the bias term. From the relation $\mathbf{X}\boldsymbol{\theta}|\mathbf{Y}, \sigma^* \sim \mathcal{N}_n(\mathbf{X}\hat{\boldsymbol{\theta}}^{\mathbb{R}}, \sigma^{*2}\mathbf{H}(a_n))$, and the posterior consistency of σ^* at σ_0 , it follows that the posterior distribution of T_j given \mathbf{Y} can be approximated arbitrarily closely in the total variation distance by $\mathcal{N}_p(m_j, \Sigma_{jj})$ uniformly for $j = 1, \dots, p$, where m_j and Σ_{jj} are respectively defined in (3.5) and (3.6). It remains to show that given the data, the bias term is asymptotically negligible, that is, for all $\epsilon > 0$, $\max_j \mathbb{P}(|\Lambda_j| > \epsilon|\mathbf{Y}) = o_P(1)$. Note that

$$\begin{aligned}
\Lambda_j & = \sqrt{n}\sum_{k \neq j} \frac{\mathbf{R}^{(j)\top}\mathbf{X}^{(k)}}{\mathbf{R}^{(j)\top}\mathbf{X}^{(j)}}(\theta_k^0 - \theta_k^*) \\
& \leq \sqrt{n}\max_{k \neq j} \left| \frac{\mathbf{R}^{(j)\top}\mathbf{X}^{(k)}}{\mathbf{R}^{(j)\top}\mathbf{X}^{(j)}} \right| \|\boldsymbol{\theta}^* - \boldsymbol{\theta}^0\|_1,
\end{aligned}$$

which can be bounded by

$$\sqrt{n}\lambda_j^{\mathbf{X}}/(2|\mathbf{R}^{(j)\top}\mathbf{X}^{(j)}/n|)\mathcal{O}_p(s_0\sqrt{(\log p)/n})$$

using the KKT condition for the LASSO of $\mathbf{X}^{(j)}$ on $\mathbf{X}^{(-j)}$ given by $|\mathbf{X}^{(k)\top}\mathbf{R}^{(j)}/n| \leq \lambda_j^{\mathbf{X}}/2$ and using Theorem 3.1. Finally, if $\lambda_j^{\mathbf{X}} = \mathcal{O}(\sqrt{(\log p)/n})$, $|\mathbf{R}^{(j)\top}\mathbf{X}^{(j)}/n|$ can be shown to be bounded away from zero (Zhang and Zhang, 2014). Consequently, $\Lambda_j = \mathcal{O}_p((s_0 \log p)/\sqrt{n})$, and choosing $s_0 = o(\sqrt{n}/\log p)$ we can prove Δ_j negligible. \square

Proof of Corollary 3.3.1. It suffices to show that the mean and variance of the approximating normal distribution of θ_j^{**} given by $\theta_j^0 + m_j/\sqrt{n}$ and Σ_{jj}/n asymptotically agree with $\hat{\theta}_j^{\text{DB}}$ and $\sigma_0^2 \|\mathbf{R}^{(j)}\|^2 / |\mathbf{X}_{(j)}^{\text{T}} \mathbf{R}^{(j)}|^2$ respectively.

Consider the singular value decomposition of the design matrix \mathbf{X} as $\mathbf{X} = \mathbf{U}\mathbf{D}\mathbf{V}^{\text{T}}$, where $\mathbf{U} \in \mathbb{R}^{n \times n}$ and $\mathbf{V} \in \mathbb{R}^{n \times p}$ satisfy $\mathbf{U}^{\text{T}}\mathbf{U} = \mathbf{I}_n$ and $\mathbf{V}^{\text{T}}\mathbf{V} = \mathbf{I}_p$, and $\mathbf{D} = \text{diag}(d_1, d_2, \dots, d_n)$, where d_1, \dots, d_n are the singular values of \mathbf{X} . Then, we have $\text{tr}(\mathbf{H}(a_n)) = \sum_{j=1}^n d_j^2 / (d_j^2 + a_n)$ and so,

$$\begin{aligned} \left| \frac{\mathbf{R}^{(j)\text{T}} \mathbf{H}(a_n) \mathbf{R}^{(j)}}{\mathbf{R}^{(j)\text{T}} \mathbf{R}^{(j)}} - 1 \right| &= \left| \frac{\mathbf{R}^{(j)\text{T}} (\mathbf{I} - \mathbf{H}(a_n)) \mathbf{R}^{(j)}}{\mathbf{R}^{(j)\text{T}} \mathbf{R}^{(j)}} \right| \\ &\leq \text{tr}(\mathbf{I}_n - \mathbf{H}(a_n)) \\ &= n \left(1 - n^{-1} \sum_{j=1}^n d_j^2 / (d_j^2 + a_n) \right) \rightarrow 0 \end{aligned}$$

by Lemma 10.1. Thus, the ratio of the variances converges to 1. Next, we show that the difference between the means of the two Gaussian distributions, normalized by the standard deviation, vanishes as n grows. By Theorem 3.3, the induced posterior distribution of $\sqrt{n}(\theta_j^{**} - \hat{\theta}_j^{\text{DB}})$ given \mathbf{Y} is approximately $\mathcal{N}_p(m_j - \sqrt{n}(\hat{\theta}_j^{\text{DB}} - \theta_j^0), \Sigma_{jj})$. Then, from Lemma 10.4, we can write

$$n^{-1/2} \frac{|\mathbf{X}^{(j)\text{T}} \mathbf{R}^{(j)}|}{\|\mathbf{R}^{(j)}\|} \left| \hat{\theta}_j^{\text{DB}} - (\theta_j^0 + m_j/\sqrt{n}) \right| \leq A_1 + A_2 = o(1),$$

where $A_1 = n^{-1/2} \|\mathbf{Y} - \mathbf{X}\hat{\boldsymbol{\theta}}^{\text{R}}\|_1 = o_P(1)$ by Lemma 10.5 and the $A_2 = n^{-1/2} \frac{\lambda^{\mathbf{X}_j/2}}{\|\mathbf{R}^{(j)}\|/n} \|\boldsymbol{\theta}^0 - \hat{\boldsymbol{\theta}}^{\text{L}}\|_1 = o_P(1)$. The latter follows as the KKT condition for the LASSO of $\mathbf{X}^{(j)}$ on $\mathbf{X}^{(-j)}$ is given by $|\mathbf{X}^{(k)\text{T}} \mathbf{R}^{(j)}|/n \leq \lambda_j^{\mathbf{X}}/2$. Finally, $\|\mathbf{R}^{(j)}\|/\sqrt{n}$ is bounded away from zero if and $s_0 \ll \sqrt{n}/(\log p)$, noting that $\|\boldsymbol{\theta}^0 - \hat{\boldsymbol{\theta}}^{\text{L}}\|_1 = \mathcal{O}_P(s_0 \lambda_n)$ from (see Theorem 6.1 in Bühlmann and van de Geer (2011)). \square

Proof of Theorem 3.4. By Theorem 3.2, with high probability, the post-variable selection posterior is supported on $\mathbb{R}^{S_0} \times \{\mathbf{0}_{S_0^c}\}$, and

$$\boldsymbol{\theta}_{S_0}^{\text{PS}} | (\mathbf{Y}, \hat{S} = S_0, \sigma) \sim \mathcal{N}_{s_0}(\hat{\boldsymbol{\theta}}_{S_0}^{\text{R,PS}}, \sigma^2 (\mathbf{X}_{S_0}^{\text{T}} \mathbf{X}_{S_0} + a_n \mathbf{I}_{s_0})^{-1}).$$

Since the post-selection setup reduces to a fixed dimensional normal regression, the marginal posterior distribution of σ is consistent. Hence, with σ integrated out, the posterior distribution of $\boldsymbol{\theta}_{S_0}^{\text{PS}}$ given $(\mathbf{Y}, \hat{S} = S_0)$ is approximated in the total variation distance by $\mathcal{N}_{s_0}(\hat{\boldsymbol{\theta}}_{S_0}^{\text{R,PS}}, \sigma_0^2 (\mathbf{X}_{S_0}^{\text{T}} \mathbf{X}_{S_0})^{-1})$, using Assumption 3.4. Consequently, by the

definition of r_α , we have as $n \rightarrow \infty$,

$$r_\alpha \rightarrow \sigma_0^2 \chi_{s_0, \alpha}^2 \text{ in } \mathbb{P}_{\theta_0}\text{-probability,} \quad (10.7)$$

where $\chi_{s_0, \alpha}^2$ is the $(1 - \alpha)$ -quantile of the chi-square distribution with s_0 degrees of freedom.

By Lemma 10.6, $\sqrt{n}(\hat{\theta}_{S_0}^{\text{R,PS}} - \theta_{S_0}^0) \rightsquigarrow \mathcal{N}_{s_0}(\mathbf{0}_{s_0}, \sigma_0^2 \mathbf{C}_{11}^{-1})$, which, together with Assumption 3.4, implies that

$$(\hat{\theta}_{S_0}^{\text{R,PS}} - \theta_{S_0}^0)^{\text{T}} (\mathbf{X}_{(1)}^{\text{T}} \mathbf{X}_{(1)} + a_n \mathbf{I}_{S_0}) (\hat{\theta}_{S_0}^{\text{R,PS}} - \theta_{S_0}^0) \rightsquigarrow \sigma_0^2 \chi_{s_0}^2.$$

Define the event

$$E_n = \{\sigma_0^2 \chi_{s_0, \alpha}^2 (1 - \delta_n) \leq r_\alpha \leq \sigma_0^2 \chi_{s_0, \alpha}^2 (1 + \delta_n)\},$$

where $\delta_n \rightarrow 0$ sufficiently slowly. Then $\mathbb{P}(E_n^c) \rightarrow 0$ as $n \rightarrow \infty$ by (10.7). On E_n , we have

$$\underline{D}_n \times \{\mathbf{0}_{S_0^c}\} \subset \{\theta_{S_0}^0 \in D_{n, 1-\alpha}^{\text{PS}}\} \subset \overline{D}_n \times \{\mathbf{0}_{S_0^c}\},$$

where

$$\begin{aligned} \underline{D}_n &= \{(\hat{\theta}_{S_0}^{\text{R}} - \theta_{S_0}^0)^{\text{T}} (\mathbf{X}_{(1)}^{\text{T}} \mathbf{X}_{(1)} + a_n \mathbf{I}_{S_0}) (\hat{\theta}_{S_0}^{\text{R}} - \theta_{S_0}^0) \\ &\quad \leq (1 - \delta_n) \sigma_0^2 \chi_{s_0, \alpha}^2\} \\ \overline{D}_n &= \{(\hat{\theta}_{S_0}^{\text{R}} - \theta_{S_0}^0)^{\text{T}} (\mathbf{X}_{(1)}^{\text{T}} \mathbf{X}_{(1)} + a_n \mathbf{I}_{S_0}) (\hat{\theta}_{S_0}^{\text{R}} - \theta_{S_0}^0) \\ &\quad \leq (1 + \delta_n) \sigma_0^2 \chi_{s_0, \alpha}^2\}. \end{aligned}$$

Thus the coverage probability $\mathbb{P}_{\theta^0}(\theta^0 \in D_{n, 1-\alpha}^{\text{PS}})$ is upper bounded by

$$\mathbb{P}_{\theta^0}(\{\theta^0 \in D_{n, 1-\alpha}^{\text{PS}}\} \cap E_n) + \mathbb{P}_{\theta^0}(E_n^c) \leq \mathbb{P}_{\theta^0}(\overline{D}_n) + \mathbb{P}_{\theta^0}(E_n^c),$$

which converges to $1 - \alpha$. Similarly, the coverage probability is lower bound by

$$\mathbb{P}_{\theta^0}(\{\theta_{S_0}^0 \in D_{n, 1-\alpha}^{\text{PS}}\} \cap E_n) - \mathbb{P}_{\theta^0}(E_n^c) \geq \mathbb{P}_{\theta^0}(\underline{D}_n) - \mathbb{P}_{\theta^0}(E_n^c),$$

which also converges to $1 - \alpha$. □

References

Muaath Ebrahim AlMansoori, Sherlyn Jemimah, Ferial Abuhantash, and Aamna Al-Shehhi. Predicting early alzheimer's with blood biomarkers and clinical features.

- Scientific Reports*, 14(1):6039, 2024.
- Artin Armagan, David B Dunson, and Jaeyong Lee. Generalized double Pareto shrinkage. *Statistica Sinica*, 23(1):119–143, 2013.
- Jincheng Bai, Qifan Song, and Guang Cheng. Nearly optimal variational inference for high dimensional regression with shrinkage priors. *arXiv preprint arXiv:2010.12887*, 2020.
- Maria Maddalena Barbieri and James O Berger. Optimal predictive model selection. *The Annals of Statistics*, 32(3):870–897, 2004.
- Eduard Belitser and Subhashis Ghosal. Empirical Bayes oracle uncertainty quantification for regression. *The Annals of Statistics*, 48(6):3113–3137, 2020.
- James O Berger and William E Strawderman. Choice of hierarchical priors: Admissibility in estimation of normal means. *The Annals of Statistics*, 24:931–951, 1996.
- Anirban Bhattacharya, Debdeep Pati, Natesh S Pillai, and David B Dunson. Dirichlet–Laplace priors for optimal shrinkage. *Journal of the American Statistical Association*, 110(512):1479–1490, 2015.
- Prithwish Bhaumik and Subhashis Ghosal. Bayesian two-step estimation in differential equation models. *Electronic Journal of Statistics*, 9(2):3124–3154, 2015.
- Prithwish Bhaumik and Subhashis Ghosal. Efficient Bayesian estimation and uncertainty quantification in ordinary differential equation models. *Bernoulli*, 23(4B):3537–3570, 2017.
- Prithwish Bhaumik, Wenli Shi, and Subhashis Ghosal. Two-step Bayesian methods for generalized regression driven by partial differential equations. *Bernoulli*, 28(3):1625–1647, 2022.
- Leo Breiman. Better subset regression using the nonnegative garrote. *Technometrics*, 37(4):373–384, 1995.
- Philip J Brown and Jim E Griffin. Inference with normal-gamma prior distributions in regression problems. *Bayesian Analysis*, 5(1):171–188, 2010.
- Peter Bühlmann and Sara van de Geer. *Statistics for High-dimensional Data: Methods, Theory and Applications*. Springer Science & Business Media, 2011.
- Peter Bühlmann, Markus Kalisch, and Lukas Meier. High-dimensional statistics with a view toward applications in biology. *Annual Review of Statistics and Its Application*, 1:255–278, 2014.

- T Tony Cai and Zijian Guo. Confidence intervals for high-dimensional linear regression: Minimax rates and adaptivity. *The Annals of Statistics*, 45(2):615–646, 2017.
- Emmanuel Candes and Terence Tao. The Dantzig selector: Statistical estimation when p is much larger than n . *The Annals of Statistics*, 35(6):2313–2351, 2007.
- Valentina Carlini, Ivan Verduci, Francesca Cianci, Gaetano Cannavale, Chiara Fenoglio, Daniela Galimberti, and Michele Mazzanti. Clic1 protein accumulates in circulating monocyte membrane during neurodegeneration. *International Journal of Molecular Sciences*, 21(4):1484, 2020.
- Carlos M. Carvalho, Nicholas G. Polson, and James G. Scott. Handling Sparsity via the Horseshoe. In David van Dyk and Max Welling, editors, *Proceedings of the Twelfth International Conference on Artificial Intelligence and Statistics*, volume 5 of *Proceedings of Machine Learning Research*, pages 73–80, Hilton Clearwater Beach Resort, Clearwater Beach, Florida USA, 2009. PMLR.
- Ismaël Castillo, Johannes Schmidt-Hieber, and Aad Van der Vaart. Bayesian linear regression with sparse priors. *The Annals of Statistics*, 43(5):1986–2018, 2015.
- Moumita Chakraborty and Subhashis Ghosal. Convergence rates for Bayesian estimation and testing in monotone regression. *Electronic Journal of Statistics*, 15(1):3478–3503, 2021a.
- Moumita Chakraborty and Subhashis Ghosal. Coverage of credible intervals in non-parametric monotone regression. *The Annals of Statistics*, 49(2):1011–1028, 2021b.
- Arindam Chatterjee and S Lahiri. Asymptotic properties of the residual bootstrap for lasso estimators. *Proceedings of the American Mathematical Society*, 138(12):4497–4509, 2010.
- Arindam Chatterjee and Soumendra Nath Lahiri. Bootstrapping lasso estimators. *Journal of the American Statistical Association*, 106(494):608–625, 2011.
- Shing Wan Choi, Timothy Shin-Heng Mak, and Paul F O’Reilly. Tutorial: a guide to performing polygenic risk score analyses. *Nature Protocols*, 15(9):2759–2772, 2020.
- Jianqing Fan and Runze Li. Variable selection via nonconcave penalized likelihood and its oracle properties. *Journal of the American Statistical Association*, 96(456):1348–1360, 2001.
- Wenjiang Fu and Keith Knight. Asymptotics for lasso-type estimators. *The Annals of Statistics*, 28(5):1356–1378, 2000.

- Tian Ge, Chia-Yen Chen, Yang Ni, Yen-Chen Anne Feng, and Jordan W Smoller. Polygenic prediction via Bayesian regression and continuous shrinkage priors. *Nature Communications*, 10(1):1776, 2019.
- Edward I George and Robert E McCulloch. Variable selection via Gibbs sampling. *Journal of the American Statistical Association*, 88(423):881–889, 1993.
- Wei Han and Yun Yang. Statistical inference in mean-field variational bayes. *arXiv preprint arXiv:1911.01525*, 2019.
- Chris Hans. Bayesian lasso regression. *Biometrika*, 96(4):835–845, 2009.
- Xichen Huang, Jin Wang, and Feng Liang. A variational algorithm for bayesian variable selection. *arXiv preprint arXiv:1602.07640*, 2016.
- Hemant Ishwaran and J Sunil Rao. Spike and slab variable selection: frequentist and Bayesian strategies. *The Annals of Statistics*, 33(2):730–773, 2005.
- Adel Javanmard and Andrea Montanari. Debiasing the lasso: Optimal sample size for Gaussian designs. *The Annals of Statistics*, 46(6A):2593–2622, 2018.
- Taesic Lee and Hyunju Lee. Prediction of alzheimer’s disease using blood gene expression data. *Scientific reports*, 10(1):3485, 2020.
- Xinzhong Li, Haiyan Wang, Jintao Long, Genhua Pan, Taigang He, Oleg Anichtchik, Robert Belshaw, Diego Albani, Paul Edison, Elaine K Green, et al. Systematic analysis and biomarker study for alzheimer’s disease. *Scientific reports*, 8(1):17394, 2018.
- Lizhen Lin and David B Dunson. Bayesian monotone regression using Gaussian process projection. *Biometrika*, 101(2):303–317, 2014.
- Timothy Shin Heng Mak, Robert Milan Porsch, Shing Wan Choi, Xueya Zhou, and Pak Chung Sham. Polygenic scores via penalized regression on summary statistics. *Genetic Epidemiology*, 41(6):469–480, 2017.
- Nicolai Meinshausen and Bin Yu. Lasso-type recovery of sparse representations for high-dimensional data. *The Annals of Statistics*, 37(1):246–270, 2009.
- Rosemary H Milton, Rosella Abeti, Stefania Averaimo, Silvia DeBiasi, Laura Vitellaro, Lele Jiang, Paul MG Curmi, Samuel N Breit, Michael R Duchon, and Michele Mazzanti. Clic1 function is required for β -amyloid-induced generation of reactive oxygen species by microglia. *Journal of Neuroscience*, 28(45):11488–11499, 2008.

- Toby J Mitchell and John J Beauchamp. Bayesian variable selection in linear regression. *Journal of the American Statistical Association*, 83(404):1023–1032, 1988.
- Sumit Mukherjee and Subhabrata Sen. Variational inference in high-dimensional linear regression. *Journal of Machine Learning Research*, 23(304):1–56, 2022.
- Richard Nickl and Sara van de Geer. Confidence sets in sparse regression. *The Annals of Statistics*, 41(6):2852–2876, 2013.
- Gaia Novarino, Cinzia Fabrizi, Raffaella Tonini, Michela A Denti, Fiorella Malchiodi-Albedi, Giuliana M Lauro, Benedetto Sacchetti, Silvia Paradisi, Arnaldo Ferroni, Paul M Curmi, et al. Involvement of the intracellular ion channel *clc1* in microglia-mediated β -amyloid-induced neurotoxicity. *Journal of Neuroscience*, 24(23):5322–5330, 2004.
- John T Ormerod, Chong You, and Samuel Müller. A variational bayes approach to variable selection. 2017.
- Samhita Pal. sparseproj. <https://github.com/SamhitaPal3/sparseProj>, 2024.
- Trevor Park and George Casella. The Bayesian lasso. *Journal of the American Statistical Association*, 103(482):681–686, 2008.
- Florian Privé, Keurcien Luu, Michael GB Blum, John J McGrath, and Bjarni J Vilhjálmsson. Efficient toolkit implementing best practices for principal component analysis of population genetic data. *Bioinformatics*, 36(16):4449–4457, 2020.
- Kolyan Ray and Botond Szabó. Variational bayes for high-dimensional linear regression with sparse priors. *Journal of the American Statistical Association*, 117(539):1270–1281, 2022.
- Diego Franco Saldana and Yang Feng. SIS: An R package for sure independence screening in ultrahigh-dimensional statistical models. *Journal of Statistical Software*, 83(2):1–25, 2018. doi: 10.18637/jss.v083.i02.
- Jun Shao and Xinwei Deng. Estimation in high-dimensional linear models with deterministic design matrices. *The Annals of Statistics*, 40:812–831, 2012.
- Qifan Song and Faming Liang. Nearly optimal Bayesian Shrinkage for High Dimensional Regression. *Science China Mathematics*, 66(2):409–442, 2017. doi: 10.1007/s11425-020-1912-6.
- Tingni Sun and Cun-Hui Zhang. Scaled sparse linear regression. *Biometrika*, 99(4): 879–898, 2012.

- Robert Tibshirani. Regression shrinkage and selection via the lasso. *Journal of the Royal Statistical Society: Series B (Statistical Methodology)*, 58(1):267–288, 1996.
- Sara van de Geer, Peter Bühlmann, Ya’acov Ritov, and Ruben Dezeure. On asymptotically optimal confidence regions and tests for high-dimensional models. *The Annals of Statistics*, 42(3):1166–1202, 2014.
- Bjarni J Vilhjálmsson, Jian Yang, Hilary K Finucane, Alexander Gusev, Sara Lindström, Stephan Ripke, Giulio Genovese, Po-Ru Loh, Gaurav Bhatia, Ron Do, et al. Modeling linkage disequilibrium increases accuracy of polygenic risk scores. *The American Journal of Human Genetics*, 97(4):576–592, 2015.
- Martin Wainwright. Sharp Thresholds for High-Dimensional and Noisy Sparsity Recovery Using-Constrained Quadratic Programming (Lasso). *Information Theory, IEEE Transactions on*, 55:2183 – 2202, 2009. doi: 10.1109/TIT.2009.2016018.
- Martin J Wainwright, Michael I Jordan, et al. Graphical models, exponential families, and variational inference. *Foundations and Trends® in Machine Learning*, 1(1–2): 1–305, 2008.
- Kang Wang and Subhashis Ghosal. Coverage of credible intervals in bayesian multivariate isotonic regression. *The Annals of Statistics*, 51:1376–1400, 2023. doi: 10.48550/arXiv.2211.12566.
- Yue Yang and Ryan Martin. Variational approximations of empirical bayes posteriors in high-dimensional linear models. *arXiv preprint arXiv:2007.15930*, 2020.
- Yun Yang, Debdeep Pati, and Anirban Bhattacharya. α -variational inference with statistical guarantees. *The Annals of Statistics*, 48(2):886–905, 2020.
- Ming Yuan and Yi Lin. Model selection and estimation in regression with grouped variables. *Journal of the Royal Statistical Society: Series B (Statistical Methodology)*, 68(1):49–67, 2006.
- Ming Yuan and Yi Lin. On the non-negative garrotte estimator. *Journal of the Royal Statistical Society: Series B (Statistical Methodology)*, 69(2):143–161, 2007.
- Bin Zhang, Chris Gaiteri, Liviu-Gabriel Bodea, Zhi Wang, Joshua McElwee, Alexei A Podtelezhnikov, Chunsheng Zhang, Tao Xie, Linh Tran, Radu Dobrin, et al. Integrated systems approach identifies genetic nodes and networks in late-onset alzheimer’s disease. *Cell*, 153(3):707–720, 2013.
- Cun-Hui Zhang. Nearly unbiased variable selection under minimax concave penalty. *The Annals of Statistics*, 38(2):894–942, 2010.

- Cun-Hui Zhang and Jian Huang. The sparsity and bias of the lasso selection in high-dimensional linear regression. *The Annals of Statistics*, 36(4):1567–1594, 2008.
- Cun-Hui Zhang and Stephanie S Zhang. Confidence intervals for low dimensional parameters in high dimensional linear models. *Journal of the Royal Statistical Society: Series B (Statistical Methodology)*, 76(1):217–242, 2014.
- Fengshuo Zhang and Chao Gao. Convergence rates of variational posterior distributions. *The Annals of Statistics*, 48(4):2180–2207, 2020.
- Yan Dora Zhang, Brian P Naughton, Howard D Bondell, and Brian J Reich. Bayesian regression using a prior on the model fit: The r2-d2 shrinkage prior. *Journal of the American Statistical Association*, 117(538):862–874, 2022.
- Hui Zou. The adaptive lasso and its oracle properties. *Journal of the American Statistical Association*, 101(476):1418–1429, 2006.